Journal of South American Earth Sciences 82 (2018) 91–107

Contents lists available at ScienceDirect

Journal of South American Earth Sciences

journal homepage: www.elsevier.com/locate/jsames

P-T evolution of metasedimentary rocks of the Santa Filomena Complex, Riacho do Pontal Orogen, Borborema Province (NE Brazil): Geothermobarometry and metamorphic modelling

Felipe H. Santos [a, b, *], Wagner S. Amaral [a], George L. Luvizotto [c], Daniel F. Martins de Sousa [a]

[a] Department of Geology and Natural Resources, Institute of Geosciences, University of Campinas, P.O. Box 6152, 13083-970, Campinas, São Paulo, Brazil
[b] Institute of Engineering and Geoscience, Federal University of Western Pará (UFOPA), 68040-255, Santarém, Pará, Brazil
[c] Department of Petrology and Metallogeny, Institute of Geoscience and Exact Science, São Paulo State University (UNESP), 13506-900, Rio Claro, São Paulo, Brazil

ARTICLE INFO

Article history:
Received 1 December 2016
Received in revised form
21 November 2017
Accepted 24 December 2017
Available online 28 December 2017

Keywords:
Santa filomena complex
Upper amphibolite facies
Brasiliano orogeny

ABSTRACT

We present in this paper petrologic data and discuss the pressure-temperature (P-T) metamorphic history of the neoproterozoic metasedimentary rocks of the Santa Filomena Complex, Riacho do Pontal Orogen, which is inserted in the southern portion of the Borborema Province (Northeast Brazil). Therefore, the data provide constraints on metamorphic evolution during Neoproterozoic Brasiliano Orogeny in Northeast Brazil. The rocks studied are aluminous schists and paragneisses. Silver-gray and red pelitic schists are intensely deformed, biotite-muscovite rich, contain centimeter-sized garnet, staurolite and kyanite porphyroblasts, and subordinately plagioclase and quartz. Paragneisses are from light gray to dark gray colored, medium to coarse-grained and display a well-spaced foliated matrix of biotite, and kyanite and garnet porphyroblasts. Locally, the schists and paragneisses are migmatized. Pressure-temperature modelling based on thermobarometric calculations indicate that metamorphism reached 643 °C with pressures estimated in 12 kbar. Pre-peak and post-peak metamorphic conditions are constrained by mineralogical and textural relationships: garnet inclusion-rich and inclusion-free (possible of higher T) are documented and the inclusion-rich core probably indicates a S_{n-1} foliation that was transposed by S_n. The pre-peak stage most probably occurred close to 500 °C and 8 kbar, in upper greenschist to lower amphibolite facies metamorphism along kyanite stability field. We also propose that post-peak stage was associated with isothermal decompression along a possible path of tectonic exhumation in conditions of 600 °C and 7 kbar. To further evaluate the equilibrium condition, pressure-temperature pseudosections were calculated for the metasedimentary rocks. Thus, the estimated metamorphic peak took place in the upper amphibolite facies. A suggested clockwise pressure-temperature path is compatible with the regional tectonic setting of continent-continent collision which occurred in the Late Neoproterozoic of Borborema Province, during the Brasiliano Orogeny.

1. Introduction

The geologic evolution of the Borborema Province has long been a matter of debate. Some authors (*e.g.*, Brito Neves et al., 2000; Santos et al., 2010; Oliveira et al., 2010; Araujo et al., 2014; Caxito et al., 2014b) support the idea that this province developed through Wilson cycles, *sensu* Murphy and Nance (2003). Other authors (Neves, 2003, 2011, 2015) hypothesize that the Borborema Province was essentially formed in the Paleoproterozoic (ca. 2.0 Ga), and since then it has remained stable as a single large continental block, where only the formation and inversion of intracontinental basins on the Archean-Paleoproterozoic basement occurred. Despite the divergences regarding the Borborema

* Corresponding author. Department of Geology and Natural Resources, Institute of Geosciences, University of Campinas, P.O. Box 6152, 13083-970, Campinas, São Paulo, Brazil.
E-mail addresses: felipeholanda@ige.unicamp.br, felipe.hds@ufopa.edu.br (F.H. Santos), wamaral@ige.unicamp.br (W.S. Amaral), george.luvizotto@gmail.com (G.L. Luvizotto), danfms@gmail.com (D.F. Martins de Sousa).

https://doi.org/10.1016/j.jsames.2017.12.013
0895-9811/

Province tectonic evolution, it is noteworthy that it occupies strategic position in western Gondwana supercontinent, and was finally established in the Late Neoproterozoic during the Brasiliano Orogeny (Brito Neves et al., 2000; Neves, 2003; Van Schmus et al., 2008; 2008). During its final structuration, when the Amazonian, São Luís/West African and São Francisco/Congo-Kasai cratons collided (Brito Neves et al., 2000; De Wit et al., 2008), orogens formed in the cratonic blocks vicinity. Five orogens were formed along the margins of the São Francisco Craton: Rio Preto, Riacho do Pontal, Sergipano, Ribeira-Araçuaí, and Brasília (Almeida et al., 1981; Alkmim, 2001).

The Riacho do Pontal Orogen, is located at the southern portion of the Borborema Province, on the northern margin of the São Francisco Craton. It is a crustal segment with a general E-W strike (Santos and Brito Neves, 1984; Bizzi et al., 2007; Uhlein et al., 2011) that was formed during a complete plate tectonic cycle in the Neoproterozoic (Caxito, 2013). Such E-W structuration is marked by strong compressive and transpressional tectonic with vergence to the São Francisco Craton (Brito Neves, 1975; Angelim, 1988; Jardim de Sá et al., 1992; Angelim and Kosin, 2001). Despite the recent advances regarding the geologic history of the Riacho do Pontal Orogen (Caxito, 2013; Caxito et al., 2014a, 2014b, 2016; Brito Neves et al., 2015, Perpetuo et al., 2016; Salgado et al., 2016), studies focusing on the tectono-metamorphic history (P-T evolution) are still scarce and deserve more consideration, because they provide valuable information on orogenetic processes (Spear et al., 2008; Brown, 2014). In this sense, we present petrographic and mineralogical data on the metamorphic evolution of the metasedimentary rocks (schists and paragneisses) of the Santa Filomena Complex in the Riacho do Pontal Orogen. Mineral assemblages and mineral chemical composition of the dominant lithotypes are presented. Furthermore, we apply several geothermobarometers in combination with metamorphic modelling via pseudosections, making it possible to discuss the P-T metamorphic history of the study area. Our results supply information for the understanding of tectonothermal evolution of the Riacho do Pontal Orogen.

2. Regional geology

2.1. The Borborema Province

The Borborema Province, which corresponds to a branched system of orogens (Brito Neves et al., 2000), is located in northeastern Brazil, north of the São Francisco Craton (Fig. 1a and b). It occupies an area of more than 450,000 km^2 (Brito Neves et al., 2000), and was initially described by Almeida et al. (1981) as one of the ten provinces that constitute the South-American Platform. In continental pre-drift paleogeographic scenarios, the Borborema Province is placed adjacent to the Nigeria, Central Africa and Cameroon provinces, and to the West Africa, Congo and São Francisco cratons (Castaing et al., 1994; Caby, 1989; Brito Neves et al., 2000; Neves, 2003; De Wit et al., 2008) (Fig. 1a). In this context, it represents the westernmost segment of the Gondwana paleocontinent (Torsvik and Cocks, 2013; Araujo et al., 2014).

The geology of the Borborema Province is diverse, and it comprehends several Archean nuclei mainly constituted by TTG orthogneisses (Fetter, 1999; Dantas et al., 2013). It presents a Palaeoproterozoic basement, formed of orthogneisses, migmatites, and supracrustal rocks. A series of Meso-to Neoproterozoic granitic intrusions, metasedimentary rocks, and shear zones (e.g., Patos, Pernambuco, Transbrasiliano, etc.) developed by the end of the Neoproterozoic (Vauchez et al., 1995; Neves and Mariano, 1999; Viegas et al., 2014). Post-shearing plutons also occur. According to Brito Neves et al. (2000), the Borborema Province may be divided into three major structural domains: (a) the Northern Domain, which includes the Médio Coreaú, Ceará Central, and Rio Grande do Norte domains; (b) the Central Domain or transversal zone, constituted of the Piancó-Alto Brígida, Alto Pajeú, Alto Moxotó, and Rio Capibaribe terrains; and (c) the Southern Domain, limited by the Pernambuco shear zone and the São Francisco Craton, respectively to the north and to the south, and includes the Riacho do Pontal and Sergipano orogens, as well as the Pernambuco-Alagoas Terrain.

2.2. The Riacho do Pontal Orogen – RPO

The Riacho do Pontal Orogen (RPO) is an E-W-trending crustal segment composed of meta-plutonic-volcano-sedimentary sequences, and associated granitoids varying from the Archean to the Late Neoproterozoic ages (Ediacaran) (Angelim and Kosin, 2001; Caxito, 2013; Caxito et al., 2014a, 2014b; Brito Neves et al., 2015). It is limited to the north by the Pernambuco shear zone and to the south by the São Francisco Craton (Fig. 1b). We adopt here the division of Oliveira (1998, 2008) and Caxito (2013) in three tectono-stratigraphic domains, from north to south: (i) Internal Domain; (ii) Central Domain; and (iii) External Domain. The Internal Domain is largely constituted of meta-volcano-sedimentary sequences of the Paulistana and Santa Filomena complexes (Angelim and Kosin, 2001). It also includes a series of meta-granitoids (Afeição Suite) (Caxito et al., 2014a), slices of the Archean/Paleoproterozoic basement, and two-mica orthogneisses (Rajada Suite). The latter occurs as sheets within the meta-volcano-sedimentary sequences. The general structural fabric of the Internal Domain is E-W. It is limited to the north by the Pernambuco shear zone, and to the south it is a thrust fault contact with the Central Domain. The Central Domain has similar geophysical characteristics to the rocks that occurred in the transition of continental and oceanic crust, and the most representative unit is the Monte Orebe Complex, which is composed of meta-volcano-sedimentary rocks, geochemically similar to ocean floor rocks (Oliveira, 2008; Caxito et al., 2014b). These characteristics indeed indicate that this domain represents remnants of a neoproterozoic oceanic crust, and marks a suture palaeo-zone (Oliveira, 1998, 2008). In the westernmost portion of the Internal Domain, the Brejo Seco meta-plutonic-volcano-sedimentary sequence crops out (Marimon, 1990; Brito Neves et al., 2015). It is constituted of meta-psammo-pelites intercalated with metatuffs, metabasalts and metarhyolites, and is intruded by a layered meta-ultramafic sequence (Salgado et al., 2016), and granitic rocks of alkaline affinity (Serra da Aldeia Suite). Caxito (2013) and Brito Neves et al. (2015) suggest that the metamorphism of the Rajada syn-colisional gneisses was generated during the Brasiliano/Panafrican Orogeny in the Late Neoproterozoic, and the intrusion of sub-alkaline to alkaline granites of the Serra da Aldeia Suite in a post-orogenic crustal relaxation phase of the orogeny (Perpetuo et al., 2016). Regarding the sedimentation age of the Santa Filomena Complex metasedimentary rocks, Brito Neves et al. (2015) and Santos et al. (2017) obtained important detrital zircon population data around 750 Ma, suggesting a maximum age of deposition in Late Neoproterozoic for the Complex.

The External Domain, limited to the south by the São Francisco Craton, is characterized by a nappe system verging towards south. It is composed of the Casa Nova Group, which is divided into two terrigenous sedimentary units, Mandacaru and Barra Bonita formations. The first, formed in a flysch-like basin, and the second in a typical shallow-marine setting (Angelim and Kosin, 2001; Caxito, 2013). In the Casa Nova Group, Brito Neves et al. (2015) found detrital zircon populations of the Cryogenian (850-635 Ma).

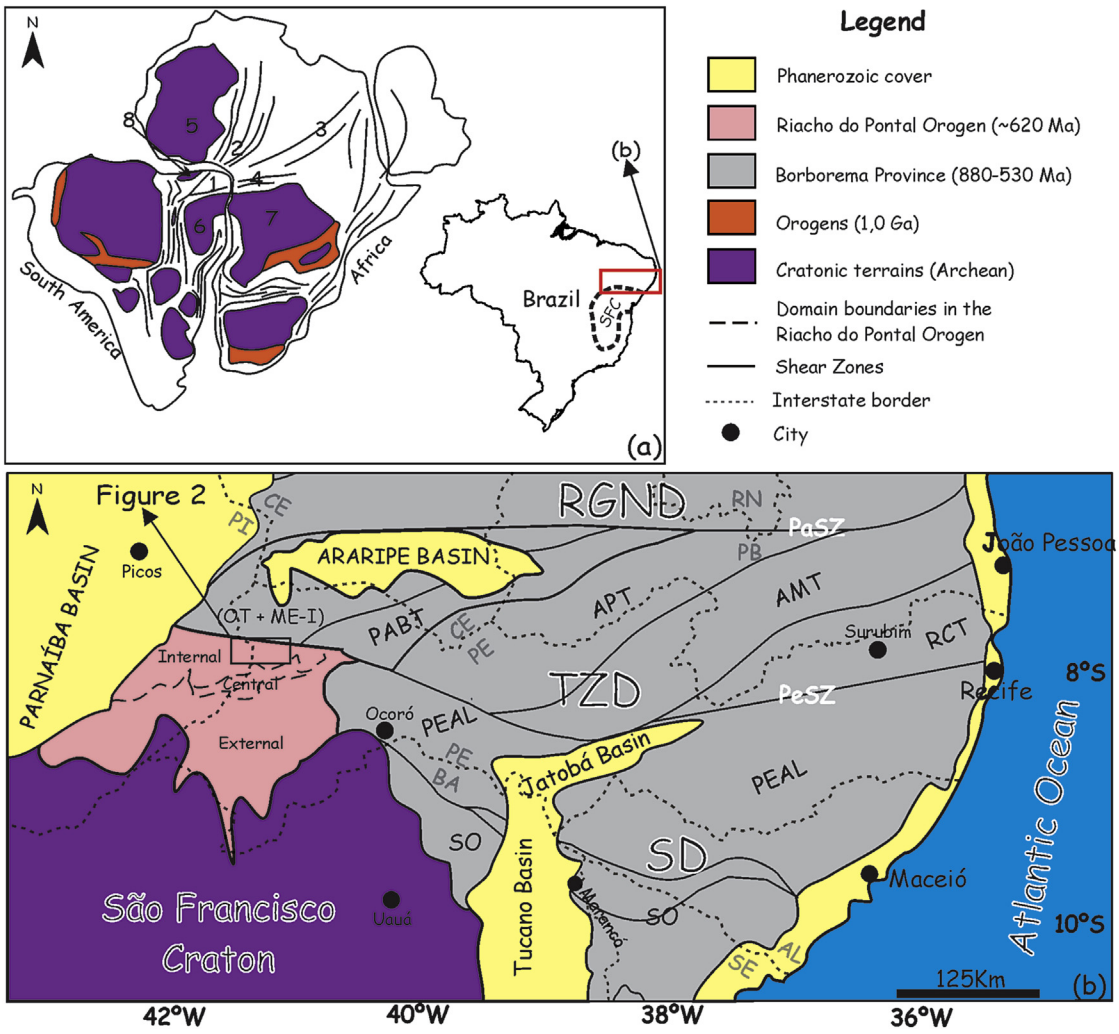

Fig. 1. Schematic geological map for West Gondwana and Borborema Province major domains. (a) West Gondwana in the Middle Paleozoic. 1 = Borborema Province; 2 = Dahomeides Orogenic System; 3 = Pharusian Orogenic System; 4 = Oubanguides Orogenic System (Central Africa); 5 = West Africa Craton; 6 = São Francisco Craton (SFC); 7 = Congo Craton; 8 = São Luís Craton. (b) Geological map of the Central Domain or Transversal Zone Domain and Southern Domain of the Borborema Province, highlighting the location of the Riacho do Pontal Orogen. RGND = Rio Grande do Norte Domain; TZD = Transversal Zone Domain; SD= Southern Domain; OT + ME-I= Ouricuri plus Morro do Estreito-Icaiçara terrains; PABT= Piancó Alto-Brígida Terrain; APT = Alto Pajeú Terrain; AMT = Alto Moxotó Terrain; RCT = Rio Capibaribe Terrain; PEAL= Pernambuco Alagoas Terrain; SO= Sergipano Orogen; PaSZ= Patos Shear Zone; PeSZ = Pernambuco Shear Zone. States of northeast Brazil: Al – Alagoas, BA – Bahia, CE – Ceará, PB – Paraíba, PE – Pernambuco, PI – Piauí, RN – Rio Grande do Norte, SE – Sergipe. Modified after Brito Neves et al. (2000), De Wit et al. (2008) and Van Schmus et al., 2008.

2.3. General geology of the Santa Filomena Complex

The Santa Filomena Complex encompasses an area of approximately 1700 km^2 and covers the whole Riacho do Pontal Orogen internal domain, including Paulistana and Betânia, Piauí and Santa Filomena, Pernambuco (Fig. 2). It is the most extensive unit of the internal domain of the Riacho do Pontal Orogen. The Santa Filomena Complex is in tectonic contact with the Afeição Suite augen-gneisses, the Rajada Suite syn-collisional gneisses, the Morro do Estreito Terrain migmatitic orthogneisses, and with the Paulistana metavolcano-sedimentary Complex. In the S-SW, between Betânia and Santa Filomena, the Santa Filomena complex is in tectonic contact with the Monte Orebe Complex. The Santa Filomena Complex is separated from the Monte Orebe Complex (Central Domain) by thrust faults.

The Santa Filomena Complex is mostly constituted of silver-gray and red pelitic schists intensively deformed with medium-to coarse-grained (Fig. 3a). These schists are biotite-muscovite rich with centimeter-sized garnet, which may reach up to 5cm in diameter, staurolite and kyanite porphyroblasts, together with plagioclase and quartz. Locally, these schists are migmatized and intercalated with migmatitic paragneisses. Melting is very incipient in the rocks, and the leucosome usually (quartz + plagioclase) occurs *in-situ* as pressure shadows around garnet and along the Sn foliation (Fig. 3b), which is defined by the alignment of biotite. The pelitic schists of Santa Filomena complex are sporadically intercalated with lenses of metamafic and metaultramafic rocks, tourmaline-bearing muscovite quartzites, tourmalinites, meta-cherts and impure calcite marbles (Fig. 3c and d). The metamafic rocks are constituted of fine-to medium-grained amphibolites.

The paragneisses described in the Santa Filomena Complex are secondary litothypes, and occurred just locally associated to the pelitic schists and Rajada leuco-gnaisses (Fig. 3e). The paragneisses are light gray to dark gray colored, medium to coarse-grained, and display a well-spaced foliated matrix composed mostly of biotite. Additionally, they contain quartz, plagioclase, muscovite, kyanite, and garnet crystals. Kyanite and garnet occurred as porphyroblasts. The rocks have widely spaced foliation defined by muscovite-

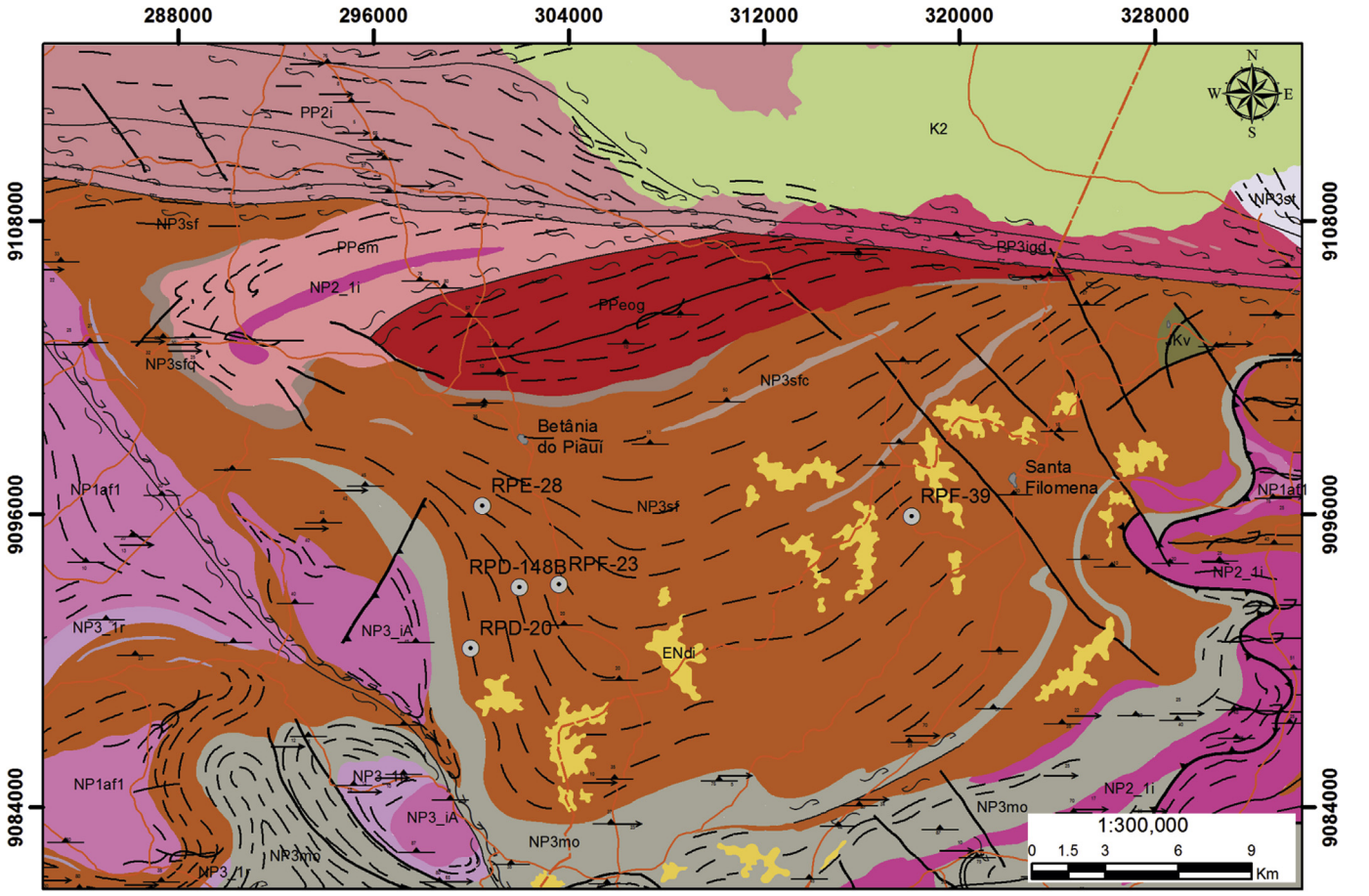

Legend

LITHOSTRATIGRAPHIC UNITS

Cenozoic

- ENdi - Dois irmãos Formation - Sandstones and conglomerates

Mesozoic

- JKv - Vale do Carir Groupi - Fine to coarse sandstones and siltstones
- K2 - Araripe Basin - Sandstones, shales and carbonates

Neoproterozoic

- NP1af1 - Afeição Suite - Augen gneisses
- NP2_1i - Indiscriminate granitoid rocks
- NP3_iA - Brasiliano age indiscriminate granitoid rocks
- NP3_1r - Rajada Suite - Orthogneisses and paragneisses
- NP3st - Santana dos Garrotes Formation
- NP3mo - Monte Orebe Complex - Metacherts, amphibolites and metapelites
- NP3sf - Santa Filomena Complex - Aluminous schists, quartz-schists, paragneisses and metavolcanic rocks
- NP3sfc - Santa Filomena Complex - Marbles
- NP3sfq - Santa Filomena Complex - Quartzites

Paleoproterozoic

- PP2i - Itaizinho Complex - Tonalitic to granodioritic orthogneisses and supracrustal rocks
- PP3igd - Icaiçara Suite
- PPem - Morro do Estreito - Migmatized orthogneisses
- PPeog - Morro do Estreito

Cartographic conventions

- Foliation
- Lineation
- Antiform
- Fracture or shear zone
- Lineament
- Sinform
- Contractional shear zone
- Extensional shear zone
- Indiscriminate shear zone
- Dextral-transcurrent shear zone
- Selected samples
- City
- State boundaries
- Access roads

Fig. 2. Simplified geological map of the eastern sector of the Santa Filomena Complex, between the Betânia, Piauí and Santa Filomena, Pernambuco, showing the locations of the selected samples for this study (Geological map adapted from Angelim, 1988).

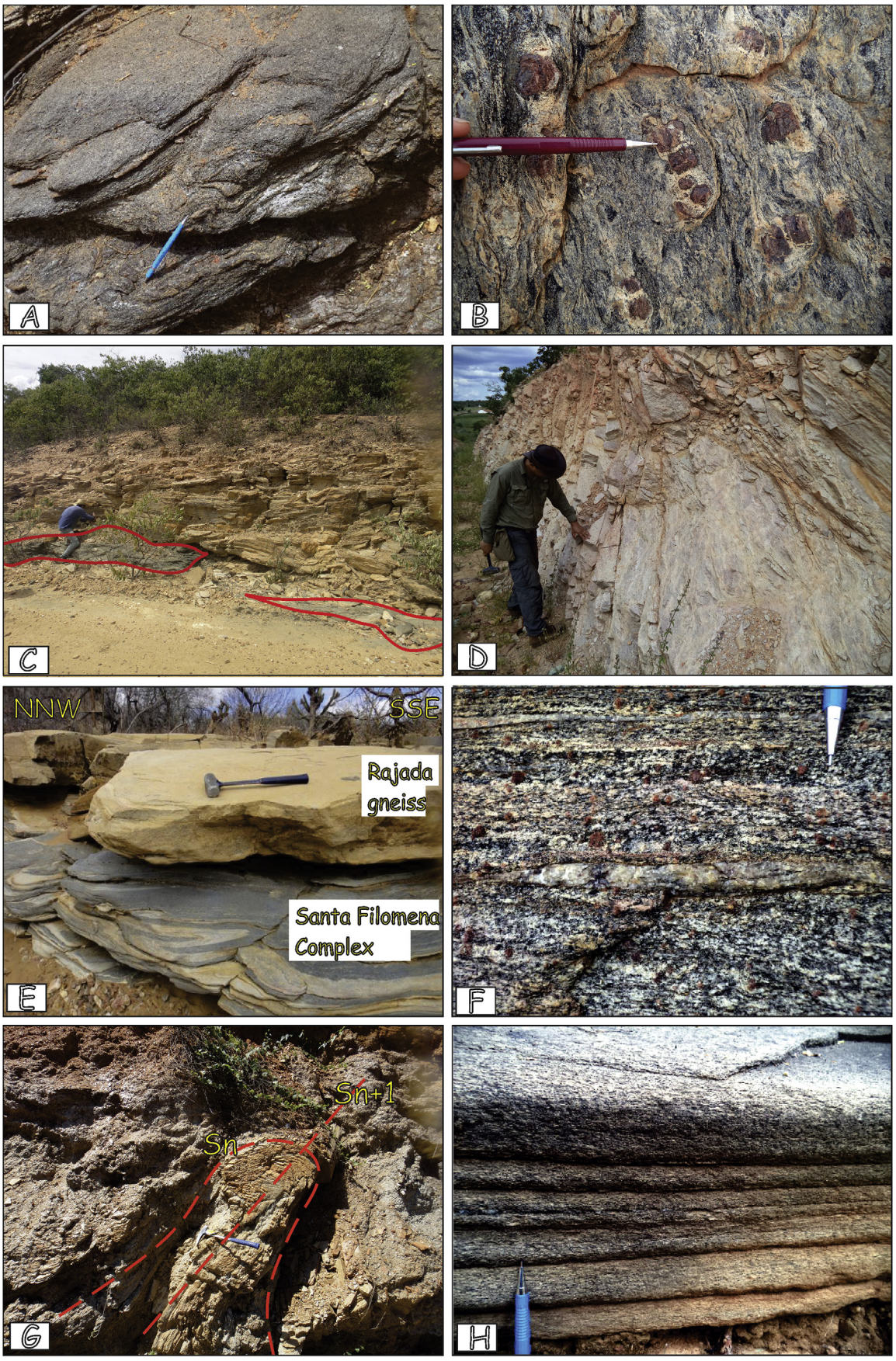
A
B
C
D
NNW
SSE
Rajada gneiss
Santa Filomena Complex
E
F
Sn+1
Sn
G
H

biotite rich layers intercalated with quartz and plagioclase rich domains. Parallel to sub-parallel to the principal foliation, as well as in schists, there are centimeter-sized garnet porphyroblasts. Locally, the semi-pelitic paragneisses are also migmatizeds, and its light-colored leucosome consists of irregular streaks and patches of coarse quartz and plagioclase with large garnet crystals (Fig. 3f). There is no presence of melanosome. The leucosome follows Sn foliation in the rock.

The regional foliation (S_n) has a NE-SW to ENE-WSW preferred orientation, with mean SE dips at variable angles. The well develop foliation or schistosity is marked by the alignment of biotite and subordinately muscovite. In the paragneiss the Sn Foliation is defined by compositional banding ($S_0//S_n$), in which irregular felsic banding is composed of quartz and plagioclase, and mafic banding, mostly by biotite. Foliation S_{n+1} occurs in schists and is represented by spaced crenulation cleavages with variable attitude and dipping to NE and SW, and axial plane to F_{n+1} inclined folds (Fig. 3g). Foliation S_{n+2} develops close to ductile shear zones (Western Pernambuco Lineament) and is a sub-vertical E-W striking mylonitic foliation. Locally (northeast of Santa Filomena), biotite-muscovite schists fine-grained with no garnet occur, showing preserved primary (S_0) bedding (Fig. 3h).

Mineral stretching lineation (L_m) is marked by the orientation of biotite, muscovite, and kyanite (when present) in the Sn foliation plane. The Lm normaly has plunging ranging from W-N-NE strikes in the central and south portion of the studied area, but closely to the basement it presents plunging to SW. Crenulation lineation (Lb) also occurs, defined by muscovite and biotite, with plunging to WSW and associated to the crenulation cleavage (S_{n+1}).

3. Petrography

The samples were collected between the Betânia and Santa Filomena, where good exposures of metasedimentary rocks (schists and paragneisses) of the Santa Filomena Complex occurs.

Below, we briefly summarize the petrographic features of representative rocks. Although we have more than six different lithologies in the study area, we selected two representative rock types (five samples), which contain mineral assemblages suitable for P–T calculations and pseudosection approach. The textural and mineralogical characteristics of the rocks are shown in Fig. 4, and mineral association in Table 1. Mineral abbreviations used in this study are according to Kretz (1983).

3.1. Staurolite-garnet-biotite schist (sample RPF-39)

This rock is characterized by the rutile-staurolite-muscovite-biotite-garnet-quartz mineral association. Foliation (Sn) is defined by the alignment of muscovite and biotite (lepidoblastic domains), alternating with richer portions in quartz and eventually plagioclase (granoblastic domains) (Fig. 4a). The representative sample RPF-39 is composed of quartz (34%), muscovite (23%), biotite (23%), plagioclase (2%), garnet (11%), staurolite (6%), and subordinate ilmenite, rutile, tourmaline and chloritoid. Quartz is the most abundant mineral and occurs as coarse-grained crystals, which sometimes show undulatory extinction. Biotite is brownish, and occurs as inclusions or replacing the garnet crystals, and in the matrix of the rock (Fig. 4b). Plagioclase crystals are medium-grained, and show irregular contacts, twinning according to the albite law, and occurs in the matrix usually associated with quartz. Garnet occurs as subidioblastic porphyroblasts with ilmenite, plagioclase, quartz, and biotite inclusions, and sometimes partially replaced by aggregates of chlorite, biotite and muscovite. Some garnet porphyroblasts display a prekinematic inclusion-free core, whereas others show irregular spiral-shaped inclusion trail, which suggests a syn-kinematic crystallization (Fig. 4c). Most garnets are oriented parallel to the Sn foliation. Staurolite crystals are xenoblastic porphyroblasts, subconcordant to the main foliation (Sn), and usually present a straight boundary with garnet. Staurolite also occurs closely connected to garnet grain, which has been partially replaced by chloritoid-biotite aggregates. Rutile is xenoblastic, in contact with biotite and muscovite, and replaces ilmenite.

3.2. Staurolite-kyanite-garnet-biotite schist (sample RPE-28)

The kyanite-garnet-muscovite-biotite schist (RPE-28) is characterized by kyanite and garnet porphyroblasts along Sn foliation (Fig. 4d). The texture is grano-lepidoblastic. Additionally, to the main foliation (S_n), it shows a S_{n+1} foliation marked by more spaced crenulation cleavage; in this case, only muscovite is present in the cleavage planes, suggesting muscovite growth in a D_{n+1} event. This sample is composed of quartz (27%), biotite (27%), muscovite (6%), garnet (19%), kyanite (15%), staurolite (5%), plus accessory minerals, such as tourmaline, chloritoid, zircon, rutile, and plagioclase. Quartz crystals are predominant in the matrix, coarse-grained, and eventually occurs as inclusion in garnet. Biotite and muscovite occur as lamellae fine-grained crystals and display two generation: the first, occurs in the matrix and is synkinematic to Sn foliation, and the youngest is post-Sn and is represented by fine flakes, which cut the earlier generations, discordant to the main foliation. Biotite also replaces garnet, kyanite, and staurolite crystals at its rims and along cracks and fractures. Minute zircon crystals (<0.01 mm) are included in biotite. Garnet occurs as subidioblastic to idioblastic porphyroblasts with poikiloblastic texture with trails of plagioclase and quartz inclusions in the core. Garnet also display an inclusion-rich core surronded by an inclusion-free rim (Fig. 4e). Additionally, some inclusions are oblique to the external foliation (Sn). Staurolite also occurs as euhedral porphyroblasts, and it is commonly in irregular contact (with subidioblastic rims) with kyanite porphyroblasts, indicating that kyanite nucleated at the expense of staurolite (Fig. 4f). Chloritoid eventually occurs in the matrix, along to the foliation, and replaces biotite, garnet, staurolite and kyanite.

3.3. Kyanite-garnet-biotite schist (samples RPF-23 and RPD-20)

This rock is staurolite free and the mineral association is kyanite-garnet-muscovite-biotite-quartz. Samples RPF-23 and RPD-20 are composed of quartz (19%), biotite (36%), muscovite (4%), garnet (22%), plagioclase (3%), kyanite (15%). Rutile, ilmenite, chloritoid, and apatite are accessories. Quartz and plagioclase occur in granoblastic lenses. Some plagioclase crystals show polysynthetic twinning and are usually replaced by biotite. Biotite is slightly brownish to strongly reddish and defines the main foliation (S_n). Garnet occurs as (up to 15 mm) porphyroblasts with poikiloblastic texture. The crystals are subidioblastic with regular to irregular rims, and are arranged parallel to the main foliation (S_n). Sometimes, in the core of the garnet crystals trails of quartz inclusions (internal foliation S_i) are oblique to the external foliation

Fig. 3. Main rocks of the Santa Filomena Complex. (a) Silver-gray pelitic schist intensively deformed with coarse-grained and biotite-muscovite rich. (b) Migmatitic schist with leucosome *in-situ* as pressure shadows around garnet and along the Sn foliation. (c) Banded aluminous schist (top) interlayered with metaultramafic rocks (bottom). (d) Tourmaline-muscovite quartzite. (e) Dark gray paragneiss of the Santa Filomena Complex in tectonic contact with Rajada syn-colisional gneiss. (f) Migmatitic paragneiss with garnet porphyroblasts and leucosome composed of quartz and plagioclase. (g) Biotite-muscovite-quartzite with inclined fold and foliation Sn+1. (h) Biotite-muscovite schist fine-grained showing preserved primary (S_0) bedding.

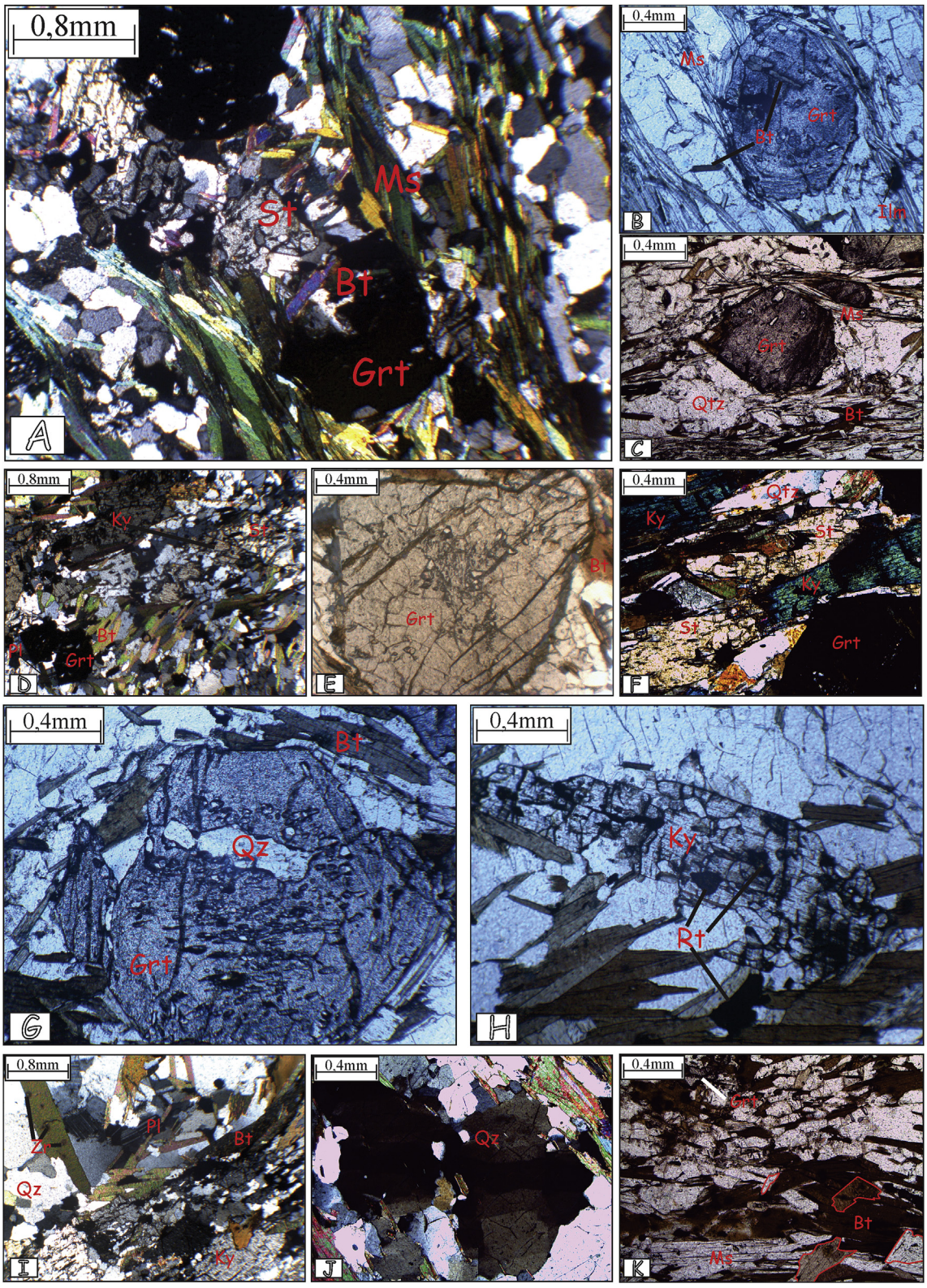

Fig. 4. Main textural and mineralogical features of the studied samples. (a), (b) and (c) Sample RPF-39; (d), (e) and (f) Sample RPE-28; (g) and (h) Sample RPF-23; (i), (j) and (k) Sample RPD-148B. (a) Photomicrograph of staurolite-garnet-muscovite-biotite schist with lepidoblastic texture and alternation with granoblastic layers (transmitted light; crossed polars). (b) Biotite inclusions in garnet. Note that in addition to biotite inclusions there are also other minerals included in core and rim of garnet (transmitted light; parallel polars). (c) Garnet porphyroblasts showing a prekinematic inclusion-free core (transmitted light; parallel polars). (d) Foliation (Sn) marked by alignment of biotite and kyanite crystals. (transmitted light; crossed polars). (e) Subdidioblastic garnet porphyroblast with plagioclase and quartz inclusions. This photomicrograph also shows an inclusion-rich core surronded by an inclusion-free garnet rim (transmitted light; parallel polars). (f) Detailed photomicrograph showing kyanite replacing staurolite (transmitted light; crossed polars). (g) Textural feature showing overgrowth of two generations of garnet: (i) inclusion-rich; and (ii) inclusion-free (transmitted light; parallel polars). (h) Kyanite porphyroblast with arrows indicating rutile inclusions (transmitted light; parallel polars). (i) Plagioclase and quartz neosome (upper side of photomicrograph) in contact with kyanite porphyroblast (transmitted light; crossed polars). (j) Photomicrograph showing chessboard extinction pattern in quartz (transmitted light; crossed polars). (k) Photomicrograph showing two

Table 1
Samples used in this study. Mineral abbreviations according to Kretz (1983).

Sample code	Rock classification	Mineral association
RPF-39	St-Grt-Bt schist	Rt-St-Ms-Bt-Grt-Qtz
RPD-148B	Ky-Grt-Bt paragneiss	Rt-Ky-Grt-Bt-Qtz
RPE-28	St-Ky-Grt-Bt schist	Rt-Ky-Pl-Grt-Bt-Qtz
RPD-20 e RPF-23	Ky-Grt-Bt schist	Rt-Ky-Pl-Grt-Bt-Qtz

(S_e), suggesting pre-tectonic (or pre-kinematic) growth in relation to S_e, and to the D_n event. The textural feature may also indicates overgrowth of two generations of some garnet crystals: (i) inclusion-rich; and (ii) inclusion-free (possible of higher temperature) (Fig. 4g). The inclusion-rich core probably indicates a S_{n-1} foliation that was transposed by S_n. Kyanite crystals. They are prismatic, subidioblastic, elongated according to foliation S_n, and contain rutile and quartz inclusions (Fig. 4h). Kyanite also is in irregular contact with plagioclase and biotite.

3.4. Kyanite -garnet-biotite gneiss (sample RPD-148)

This rock is constituted of quartz (33%), biotite (27%), muscovite (9%), garnet (23%), plagioclase (1%), kyanite (6%). Zircon, apatite, tourmaline, rutile, and ilmenite are accessories. Quartz shows undulatory extinction, it is recrystallized in sub-grains, forming continuous granoblastic lenses (leucosome) with plagioclase, and often displays a chessboard pattern of extinction (Fig. 4i and j). Biotite and muscovite form lepidoblastic lenses intercalated with granoblastic segments and define foliation S_n. The foliation is usually anastomosed, surround garnet porphyroblasts, and represent a tardi-peak metamorphic stage. Brownish biotite occurs in lamellae with rutile and zircon inclusions, and it sometimes replaces garnet and kyanite at its rims. In general, biotite shows three generations. The first occurs as inclusion in garnet and kyanite; the second associated with S_n foliation, and the third and the youngest, with muscovite, as it randomly agglomerates that cut S_n (post-peak), and replaces the garnet and kyanite porphyroblasts (Fig. 4k). Garnet porphyroblasts may be centimeter sized, and show subidioblastic and poikiloblastic texture with quartz, plagioclase, biotite and ilmenite inclusions in its core. The inclusions occur parallel to the external foliation and are pre-peak metamorphic phases. Kyanite occurs as xenoblastic to subidioblastic porphyroblasts. It may be deformed, and contains quartz, biotite, rutile, and tourmaline inclusions, and it is partially replaced by muscovite and biotite. When it occurs, kyanite rims are very irregular and muscovite and biotite do not follow S_n. Eventually, kyanite occurs as prismatic agglomerates in the matrix.

4. Mineral chemistry

Mineral chemical analyses were performed at the Department of Petrology and Metalogeny, São Paulo State University – UNESP, using a JEOL JXA-8230 Electron Microprobe, equipped with five WDS spectrometers (PET, TAP, LDE1, LDE2, and LIF crystals), EDS detector, cathodoluminescence detector, and secondary and backscattered electron detectors. Operating conditions were set to 15 kV and 10-20 nA. Rutile trace element (Si, Al, Cr, Sb, Sn, W, Ta, Hf, Fe, Nb and Zr) analyses were carried out using 20 kV and 80 nA, and followed the settings of Luvizotto et al. (2009). Counting time for the major elements was 10 s in the peak position, and 5 s in background position. For the trace elements, counting time was 20 s in peak position, and 10 s in background position.

Representative analyses of garnet, biotite, muscovite, plagioclase, and rutile are listed in Tables 2–5, respectively.

4.1. Garnet

Garnet grains are generally 2–8 mm euhedral to subhedral porphyroblasts, with mineral inclusions such as biotite, plagioclase, muscovite, quartz, rutile and ilmenite, and surrounded mainly by biotite, plagioclase, and quartz. Two domains in garnet were analyzed according to the textural characteristics: (i) garnet cores with inclusions; and (ii) garnet rim in contact with biotite, muscovite, and kyanite. In general, the garnet core showed similar chemical variation in all samples, whereas the rim, a different pattern in relation to the core. The composition of the analyzed garnet is mainly XAlm (0.557–0.737) and XGrs (0.029–0.230), and secondarily XSps (0.012–0.143), XPrp (0.047–0.146), and XAdr (0.011–0.029) (Table 2 and Fig. 5). There is a considerable increase from 0.557 to 0.737 of the almandine molecule XAlm [$(Fe^{2+}/(Fe^{2+} + Mn + Mg + Ca)$], from core to rim. Regarding the grossular and spessartine molecules, [XGrs = $(Ca\text{-}3Adr)/(Fe^{2+} + Mn + Mg + Ca)$] and [XSps = $Mn/(Fe^{2+}+Mn + Mg + Ca)$], respectively, the opposite process occurs with a decrease from the core to rim. Additionally, the analyzed garnets show a decrease, from core to rim, of XFe [$Fe^{2+}/(Fe^{2+} + Mg) = 0.925–0.863$] and XCa [$Ca/(Ca + Fe^{2+}+Mg) = 0.276–0.052$). Besides the molar fraction variations, some rim of garnet-bearing samples showed higher values in pyrope and almandine molecule than others samples. The sample RPE-28, for instance, showed XPrp = .146. The variations in the molar fractions of some components may be better visualized in Fig. 5. The results of chemical analyses are presented in Table 2.

4.2. Biotite

Two main textures of biotite were recognized: (i) biotite as inclusion in garnet, and (ii) biotite in contact with garnet, staurolite, and kyanite in the matrix of the rock. Despite the textural distinction, detailed compositional individualization was not possible, due to some inclusions yielded compositions almost identical to those of biotite in contact with aluminosilicates. For example, FeO (19.93 wt%) and MgO contents (10.78 wt%) obtained for the core of biotite inclusions in garnet from sample RPF-39 were very close to those obtained for sample RPD-148B (19.94 wt% FeO and 10.45 wt% MgO). On the other hand, two biotite groups are characterized by means of TiO_2, FeO and MgO contents. For the first group, contents of TiO_2 are 1.30–1.86 wt%, FeO 16.52–16.91 wt%, and MgO 8.57–10.78 wt%. Basically, the first biotite group occurred in the matrix, and it is concordant to Sn foliation, and in contact with staurolite. The second group yielded higher TiO_2 (1.91–2.85 wt%), FeO (20.31–22.59 wt%), and MgO (12.83–12.98 wt%) contents. This group is composed of biotite in contact with kyanite and garnet crystals. The results of biotite chemical analyses are presented in Table 3.

4.3. Muscovite

Muscovite was analyzed from samples RPD-148B and RPE-28. Small variations of FeO and MgO contents were observed, respectively 0.79–0.99 wt% and 0.53–0.69 wt%, with the exception of a discordant muscovite from foliation S_n, which yielded the highest FeO (1.19 wt%), and MgO contents (0.87 wt%). For sample RPD-148B,

generations of biotite and muscovite. Note the youngest (highlighted in red outline), that cut Sn, and replaces the garnet and kyanite (transmitted light; parallel polars). (For interpretation of the references to color in this figure legend, the reader is referred to the Web version of this article.)

Table 2
Representative chemical analyses of garnets. Structural formula calculated on the basis of 12 oxygens.

Rock	Ky-Grt-Bt schist						St-Grt-Bt schist		Ky-Grt-Bt paragneiss	St-Ky-Grt-Bt schist		
Sample	RPD-20	RPD-20	RPD-20	RPD-20	RPF-23	RPF-23	RPF-39	RPF-39	RPD-148b	RPE-28	RPE-28	RPE-28
Texture	Core	Rim	Core	Rim	Core	Core	Rim	Rim	Rim	Core	Rim	Rim
SiO_2	36.53	36.62	36.81	36.23	36.26	36.35	36.12	36.55	36.67	36.58	36.36	36.10
TiO_2	0.01	0.01	0.05	0.00	0.52	0.07	0.26	0.09	0.05	0.10	0.03	0.00
Al_2O_3	21.01	20.63	20.78	20.76	21.02	21.14	20.76	20.68	21.34	21.08	21.40	21.33
Cr_2O_3	0.00	0.00	0.02	0.00	0.02	0.00	0.03	0.00	0.00	0.02	0.01	0.00
Fe_2O_3	0.35	0.61	0.78	0.65	0.72	0.49	0.77	0.88	0.65	0.58	0.61	0.97
FeO	25.51	33.00	26.25	33.55	31.86	26.22	32.94	27.54	30.60	29.44	33.45	32.70
MnO	6.23	3.88	4.98	3.98	2.64	5.53	0.65	4.33	0.54	3.84	0.79	1.37
MgO	1.17	2.63	1.54	2.67	2.72	1.40	3.00	1.18	1.77	1.73	3.65	2.78
CaO	8.32	2.21	8.54	1.67	4.47	8.21	4.49	8.45	8.70	6.71	3.57	5.07
Na_2O	0.00	0.00	0.03	0.01	0.00	0.00	0.02	0.04	0.02	0.05	0.01	0.03
K_2O	0.00	0.00	0.00	0.00	0.00	0.01	0.02	0.00	0.00	0.00	0.00	0.00
Total	99.14	99.59	99.78	99.53	100.23	99.42	99.06	99.74	100.35	100.13	99.88	100.35
Si	2.967	2.982	2.971	2.960	2.925	2.946	2.942	2.964	2.940	2.952	2.929	2.913
Ti	0.000	0.001	0.003	0.000	0.032	0.004	0.016	0.005	0.003	0.006	0.002	0.000
Al	2.011	1.980	1.977	1.999	1.999	2.020	1.993	1.977	2.017	2.005	2.032	2.029
Cr	0.000	0.000	0.001	0.000	0.001	0.000	0.002	0.000	0.000	0.001	0.001	0.000
Fe^{3+}	0.000	0.000	0.000	0.000	0.000	0.000	0.000	0.000	0.000	0.000	0.000	0.000
Fe^{2+}	1.754	2.285	1.819	2.333	2.193	1.807	2.291	1.921	2.092	2.022	2.290	2.265
Mn	0.428	0.268	0.341	0.275	0.180	0.380	0.045	0.297	0.037	0.263	0.054	0.094
Mg	0.142	0.319	0.185	0.325	0.327	0.169	0.364	0.143	0.212	0.208	0.438	0.334
Ca	0.724	0.193	0.739	0.146	0.386	0.713	0.392	0.734	0.748	0.580	0.308	0.438
Adr	0.011	0.019	0.024	0.020	0.022	0.015	0.024	0.027	0.020	0.017	0.019	0.029
Prp	0.047	0.106	0.062	0.108	0.109	0.056	0.121	0.047	0.070	0.069	0.146	0.111
Sps	0.143	0.089	0.113	0.092	0.060	0.126	0.015	0.099	0.012	0.087	0.018	0.031
Grs	0.230	0.046	0.221	0.029	0.106	0.223	0.106	0.217	0.229	0.175	0.084	0.116
Alm	0.557	0.733	0.568	0.737	0.676	0.561	0.712	0.595	0.647	0.633	0.708	0.680
X_{Fe}	0.925	0.877	0.908	0.878	0.870	0.914	0.863	0.931	0.908	0.907	0.839	0.871
X_{Ca}	0.276	0.069	0.269	0.052	0.133	0.265	0.129	0.262	0.245	0.206	0.101	0.144

Na_2O, and K_2O contents varied between 0.88 and 0.96 wt% and 9.33–9.37 wt%, respectively, whereas for sample RPE-28, Na_2O contents were a little higher in the range of 1.97–2.11 wt%, and K_2O contents a little lower (7.44–7.59 wt%). Muscovite chemical analyses are listed in Table 4.

4.4. Plagioclase

Plagioclase cores and rims were analyzed. With exception of the plagioclase from sample RPF-39, a slight increase in anorthite (An) was observed from core to rim (Table 4). The plagioclase chemical compositions are close to those of oligoclase (90-70% Ab).

4.5. Rutile

Rutile crystals from samples RPD-20 and RPF-23 were analyzed. Crystal sizes vary from *ca.* 50 μm to 100μm. Rutile grains are subidioblastic and occur as inclusions in kyanite and garnet (Figs. 4f and 6). Trace element chemical composition of the analyzed grains is presented in Table 5. Low Si contents obtained for all spots indicate contamination free analyses, and may be used as a quality control. Low Cr content, in respect to Nb, confirms the felsic nature of the rocks (Zack et al., 2004). High Nb contents (up to 8600 ppm for sample RDP20) may be due to rutile growth from biotite breakdown, as suggested by Luvizotto and Zack (2009). Zr contents in rutiles from sample RPF-23 vary from 192 to 204 ppm, and are slightly lower than in sample RPD-20 (300-330 ppm). The scattering of data within each sample is small and no significant variation in composition is observed when more than one spot is analyzed in each grain.

5. P-T metamorphic conditions

Metamorphic conditions were estimated from: (a) conventional thermobarometric models with the aid of GPT Excel spreadsheet (Reche and Martinez, 1996); (b) an internally-consistent thermodynamic databank offered by winTWQ software, version 2.32 (Berman, 1988, 1991, 2007); (c) Zr thermometry applied to rutile; and (d) P-T pseudosections, prepared with PERPLE_X software (Connolly, 2005; available on http://www.perplex.ethz.ch/).

5.1. Geothermobarometry

Estimated pressure and temperature values for the selected samples, using conventional thermobarometers, are presented in Table 6. Temperatures were calculated by using the garnet-biotite (Grt-Bt) thermometer (based on the Fe-Mg cationic exchange between garnet and biotite), and pressures with the garnet-kyanite-plagioclase-quartz (GASP), and garnet-muscovite-biotite-kyanite (GMBA) barometers. The models proposed by Thompson (1976), Holdaway and Lee (1977), Hodges and Spear (1982), Ganguly and Saxena (1984), and Indares and Martignole (1985) were applied to samples RPD-20, RPF-23, RPD-148B, RPF-39, and RPE-28 with mean values of 615 °C, 648 °C, 523 °C, 496 °C and 535 °C, respectively.

Regarding geobarometry, the calibrations proposed by Newton and Haselton (1981), Hodges and Spear (1982), Ganguly and Saxena (1984), Hodges and Crowley (1985), Koziol (1989) and Holdaway et al. (1988) were applied. Differently for other samples, Holdaway et al. (1988) calibration was used for the mineral assemblage garnet-muscovite-biotite-kyanite from sample RPE-28 only, because in this sample plagioclase is more scarce, and GASP could not be applied (Table 6). The maximum variation for the

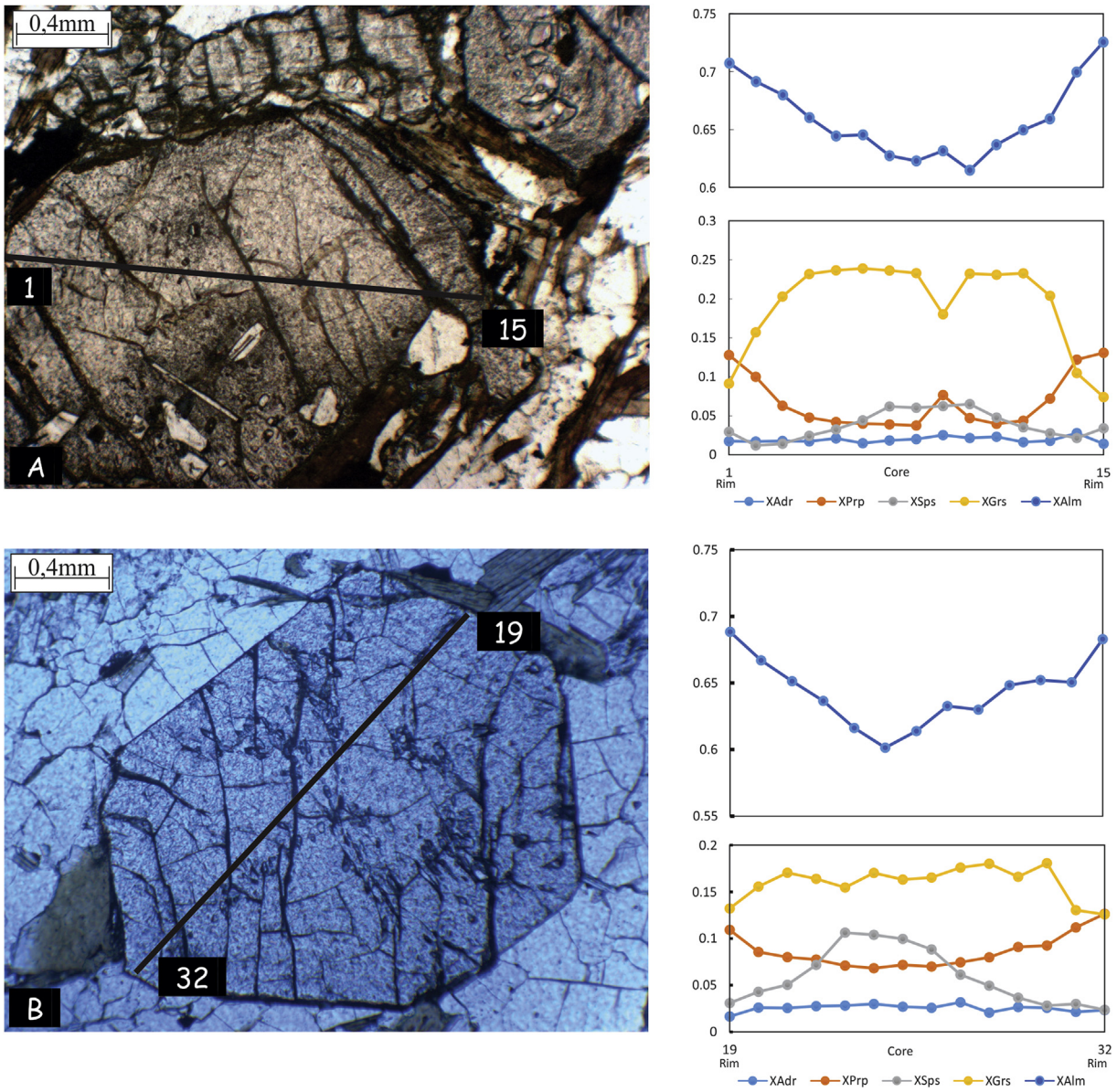

Fig. 5. Profiles of analyzed garnet. (a) Profile for the sample RPF-23. Notice the decrease, from core to rim, in grossular molecule. Pyrope and almandine molecules display an increase from core to rim. (b) Profile for the sample RPE-38. Notice the slight decrease, from core to rim, in sperssartine molecule and an increase in almandine.

pressures was of the order of 1.7 kbar, obtained for sample RPD-148B. Estimated temperature and pressure variations may be due to different activity models (activity composition relations), and different thermodynamic data used in these studies.

The P-T conditions for the equilibrium reactions were estimated using the winTWQ software (version 2.32). From the end members among the mineral phases present in a specific P-T range, the program calculated the possible (stable and meta-stable) equilibrium curves applicable to the sample. The end members for the calculations were almandine, annite, albite, anorthite, grossular, kyanite, phlogopite, pyrope, alpha-quartz, staurolite, chlorite, and muscovite.

The winTWQ software produced 2 to 4 possible equilibrium conditions for the mineral assemblages selected for each sample. The P-T calculations suggested equilibrium conditions at 495 °C and 9.1 kbar for RPF-39 (Fig. 7a); 470 °C and 7.7 kbar for sample RPD-148B (Fig. 7b); 573 °C and 10.1 kbar for sample RPE-28 (Fig. 7c); 605 °C and 7.2 kbar for sample RPD-20 (Fig. 7d), and 643 °C and 11.8 kbar for sample RPF-23 (Fig. 7e).

Rutile was relatively frequent as inclusions in garnet and kyanite porphyroblasts in samples RPD-20 and RPF-23 (Fig. 6), and were represented by the mineral assemblage kyanite-plagioclase-garnet-muscovite-biotite, and P-T conditions of the order of 605 °C-7.2 kbar and 643 °C-11.8 kbar, respectively (see Fig. 7d and e). The Zr-in-rutile geothermometer was also applied to these samples. Calculations using calibration of Tomkins et al. (2007) (Table 5), and values of pressures of 7.2 kbar for sample RPD-20, and 11.8 kbar for sample RPD-23 (winTWQ results) yielding temperatures of ca. 640 and 625 °C, for samples RDP20 and 23, respectively. The results agreed within error with calculations obtained by other geothermometers.

5.2. P-T pseudosections

P-T pseudosections were calculated for two samples (RPF-23 and RPE-28), using the PERPLE_X software (Connolly, 2005), in the

Table 3
Representative chemical analyses of biotite. Structural formula calculated on the basis of 11 oxygens.

Rock	Ky-Grt-Bt schist							St-Grt-Bt schist	Ky-Grt-Bt paragneiss	St-Ky-Grt-Bt schist		
Sample	RPD-20	RPD-20	RPD-20	RPD-20	RPF-23	RPF-23	RPF-23	RPF-39	RPD-148B	RPE-28	RPE-28	RPE-28
Texture	Core	Core	Core	Core	Inclusion	Core	Core	Inclusion	Core	Core	Core	Core
SiO_2	34.90	34.68	35.04	34.92	35.50	35.20	35.84	35.53	36.04	36.78	36.98	37.10
TiO_2	2.85	1.91	2.31	1.92	2.02	1.86	2.08	1.30	1.86	1.47	1.50	1.42
Al_2O_3	19.56	20.21	19.59	19.87	19.74	19.26	20.22	20.33	19.94	19.45	19.71	19.61
Cr_2O_3	0.03	0.04	0.02	0.04	0.03	0.04	0.05	0.03	0.02	0.04	0.01	0.04
FeO	22.59	21.74	22.54	22.10	21.03	20.31	21.29	19.83	19.94	16.52	17.53	16.91
MnO	0.08	0.08	0.09	0.66	0.09	0.05	0.08	0.29	0.08	0.01	0.01	0.00
MgO	8.57	9.27	9.04	9.22	9.70	10.55	9.39	10.78	10.45	12.98	12.83	12.97
Na_2O	0.22	0.21	0.24	0.23	0.17	0.17	0.16	0.16	0.20	0.22	0.10	0.18
K_2O	8.34	8.57	8.65	8.47	8.38	7.97	8.39	8.52	8.75	8.30	8.07	8.46
BaO	0.19	0.22	0.22	0.21	0.18	0.19	0.17	0.10	0.11	0.14	0.11	0.10
Total	97.33	96.92	97.73	97.64	96.84	95.61	97.66	96.85	97.37	95.91	96.83	96.79
Si	2.629	2.616	2.632	2.624	2.663	2.663	2.663	2.650	2.674	2.716	2.710	2.718
Ti	0.162	0.108	0.131	0.108	0.114	0.106	0.116	0.073	0.104	0.082	0.082	0.078
Al	1.736	1.797	1.734	1.760	1.745	1.717	1.770	1.787	1.743	1.693	1.702	1.693
Cr	0.002	0.002	0.001	0.002	0.002	0.002	0.003	0.001	0.001	0.002	0.000	0.002
Fe^{2+}	1.423	1.371	1.416	1.389	1.319	1.285	1.323	1.237	1.237	1.020	1.074	1.036
Mn	0.005	0.005	0.006	0.042	0.006	0.003	0.005	0.018	0.005	0.001	0.001	0.000
Mg	0.962	1.042	1.012	1.033	1.084	1.190	1.040	1.198	1.155	1.429	1.401	1.416
Ca	0.000	0.000	0.000	0.000	0.000	0.000	0.000	0.000	0.000	0.000	0.000	0.000
Na	0.032	0.031	0.035	0.034	0.025	0.025	0.022	0.023	0.028	0.032	0.014	0.026
K	0.802	0.825	0.829	0.812	0.801	0.769	0.795	0.810	0.828	0.782	0.754	0.790
Ba	0.006	0.006	0.006	0.006	0.005	0.006	0.005	0.003	0.003	0.004	0.003	0.003
X_{Fe}	0.597	0.568	0.583	0.574	0.549	0.519	0.560	0.508	0.517	0.417	0.434	0.422

Table 4
Representative chemical analyses of plagioclase and muscovite. Structural formula calculated on the basis of 8 oxygens for plagioclase and 11 oxygens and for muscovite.

Rock	Ky-Grt-Bt schist					St-Grt-Bt schist		Ky-Grt-Bt paragneiss			St-Ky-Grt-Bt schist	
Sample	RPD-20	RPD-20	RPF-23	RPF-23	RPF-23	RPF-39	RPF-39	RPD-148B	RPD-148B	RPD-148B	RPE-28	RPE-28
Mineral	Pl	Pl	Pl	Pl	Pl	Pl	Pl	Pl	Mus	Mus	Mus	Mus
Texture	Core	Core	Core	Rim	Rim	Core	Rim	Rim	Inclusion	Core	Core	Core
SiO_2	63.21	60.19	63.90	62.58	60.30	63.05	64.58	61.69	46.59	46.46	46.24	45.89
TiO_2	0.00	0.00	0.00	0.00	0.00	0.00	0.00	0.00	0.64	0.79	0.41	0.33
Al_2O_3	23.01	24.92	22.86	23.80	25.56	22.91	22.04	24.67	36.14	36.82	36.73	37.28
Cr_2O_3	0.00	0.00	0.00	0.00	0.00	0.00	0.00	0.00	0.04	0.03	0.02	0.02
FeO	0.03	0.06	0.02	0.09	0.03	0.02	0.02	0.20	1.19	0.99	0.87	0.79
MnO	0.00	0.00	0.00	0.00	0.00	0.00	0.00	0.00	0.02	0.00	0.01	0.02
MgO	0.00	0.00	0.00	0.00	0.00	0.00	0.00	0.00	0.87	0.66	0.69	0.53
CaO	3.57	6.00	3.57	4.57	6.46	3.41	2.61	5.66	0.00	0.00	0.00	0.00
Na_2O	9.38	8.17	9.70	8.82	7.84	9.71	10.08	8.51	0.88	0.96	1.97	2.11
K_2O	0.13	0.06	0.08	0.07	0.07	0.06	0.06	0.05	9.33	9.37	7.59	7.44
BaO	0.00	0.00	0.00	0.00	0.00	0.00	0.00	0.00	0.28	0.26	0.32	0.33
Total	99.34	99.40	100.13	99.93	100.26	99.15	99.40	100.78	95.97	96.35	94.86	94.74
Si	2.808	2.692	2.817	2.770	2.675	2.807	2.858	2.720	3.063	3.041	3.051	3.030
Ti	0.000	0.000	0.000	0.000	0.000	0.000	0.000	0.000	0.032	0.039	0.020	0.016
Al	1.205	1.313	1.187	1.241	1.336	1.202	1.150	1.282	2.800	2.840	2.857	2.901
Cr	0.000	0.000	0.000	0.000	0.000	0.000	0.000	0.000	0.002	0.002	0.001	0.001
Fe^{2+}	0.001	0.001	0.000	0.002	0.001	0.000	0.000	0.004	0.065	0.054	0.048	0.044
Mn	0.000	0.000	0.000	0.000	0.000	0.000	0.000	0.000	0.001	0.000	0.001	0.001
Mg	0.000	0.000	0.000	0.000	0.000	0.000	0.000	0.000	0.085	0.064	0.068	0.052
Ca	0.170	0.288	0.169	0.217	0.307	0.163	0.124	0.267	0.000	0.000	0.000	0.000
Na	0.808	0.709	0.829	0.757	0.674	0.838	0.865	0.727	0.112	0.122	0.252	0.270
K	0.008	0.003	0.005	0.004	0.004	0.003	0.003	0.003	0.783	0.782	0.639	0.626
Ba									0.007	0.007	0.008	0.008
X_{Fe}									0.434	0.457	0.412	0.457
An (%)	17.3	28.8	16.8	22.2	31.2	16.2	12.5	26.8				
Ab (%)	82.0	70.9	82.7	77.4	68.4	83.5	87.2	72.9				
Or (%)	0.8	0.3	0.5	0.4	0.4	0.3	0.3	0.3				

interval from 7.0 to 13 kbar (RPF-23) and 6.0–14 kbar (RPE-28), both within the 500-700 °C temperature range (Fig. 8). It was necessary to use a thermodynamics data bank internally consistent for minerals and fluids to accomplish them (CORK model, Holland and Powell, 1991, 1998). The following solid solution models were included (a-X): Bio(HP) for biotite, St (HP) for staurolite, Ctd (HP) for chloritoid, Gt (HP) for garnet, Mica (CF) for muscovite, Pl (I1, HP) for plagioclase, and ilm (WPH) for ilmenite. As melting is very restricted in the study area (sample RPD-148B), we did not include specific solid solution models for these situations. The whole rock

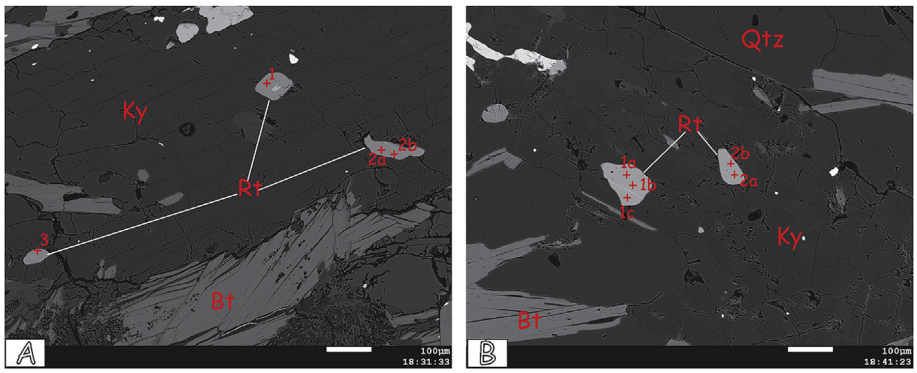

Fig. 6. BSE images of analyzed rutile. Rutile crystals are included in kyanite. Analyzed spots are shown in the figures (a) Sample RPD-20. (b) Sample RPF-23.

Table 5
Representative chemical analyses of the rutile. Values in ppm. Bd = Below detection. Temperatures are calculated using a pressure of 7.2 kbar for sample RPD-20 and 11.8 kbar for sample RPF-23.

Rock	Kyanite-garnet-biotite schist								
Sample	RPD 20_Rt1	RPD 20_Rt2a	RPD 20_Rt2b	RPD 20_Rt3	RPF 23_Rt1a	RPF 23_Rt1b	RPF 23_Rt1c	RPF 23_Rt2a	RPF 23_Rt2b
Si	28	47	42	56	28	379	402	47	65
Al	286	339	339	360	191	169	233	222	275
Cr	817	547	547	522	485	473	473	565	516
Sb	Bd	bd	Bd	Bd	bd	14	bd	bd	Bd
Sn	158	208	117	125	167	150	100	175	192
W	147	442	Bd	66	106	bd	287	41	90
Ta	194	280	295	Bd	101	93	194	54	210
Hf	Bd	32	Bd	Bd	bd	bd	bd	bd	Bd
Fe	3646	3629	3875	4511	2366	bd	2730	1950	1916
Nb	3691	5641	5746	8612	3537	3551	3936	3369	3258
Zr	330	306	300	300	192	198	204	192	198
Temperature (°C); cf. Tomkins et al., 2007	645	639	638	638	622	625	627	622	625

Table 6
Calculated P-T values using the GPT worksheet (Reche and Martinez, 1996).

Samples	RPF-39	RPD-148B	RPE-28	RPD-20	RPF-23
Models					
Geothermometry	T (°C)	T (°C)	T (°C)	T (°C)	T (°C)
Garnet-Biotite thermometer					
Thompson, 1976	447	500	564	618	637
Holdaway and Lee, 1977	434	487	538	592	600
Hodges and Spear, 1982	457	532	552	614	653
Ganguly and Saxena, 1984	457	504	480	604	617
Indares and Martignole, 1985-2	496	523	535	615	648
Average	458.2	509.2	533.8	608.6	631
Geobarometry	P (kbar)	P (kbar)	P (kbar)	P (kbar)	P (kbar)
Garnet-plagioclase-kyanite-quartz barometer					
Newton and Haselton, 1981	10.2	7.5	–	8.2	11.8
Hodges and Spear, 1982	9.8	7.8	–	7.2	10.8
Ganguly and Saxena, 1984	11.3	9.2	–	6.6	11.3
Hodges and Crowley, 1985	10.6	8.4	–	7.6	12
Koziol, 1989	11	8.2	–	8.7	12
Average	10.58	8.22	–	7.66	11.58
Garnet-muscovite-biotite-kyanite barometer					
Holdaway et al., 1988			10,2		

chemical composition (bulk composition) was obtained by the ICP-ES method (Spectro Ciros Vision) in ACME Analytical Laboratories Ltd. Vancouver, Canada.

Calculations were carried out in the Na_2O-CaO-K_2O-FeO-MgO-Al_2O_3-SiO_2-H_2O-TiO_2 chemical system (NCKFMASHT). Oxygen was not included, since magnetite was not identified in thin section, and the amount of ferric iron in the analyzed samples was low. The NCKFMASHT chemical system represented the mineral associations found in the meta-psammo-pelites with reasonable precision. In all pseudosections, water (H_2O) was considered in excess, due to the occurrence of phyllosilicates in the samples.

Pseudosections calculated for RPF-23 and RPE-28 are constituted of bi- and trivariant fields (Fig. 8a and b), and contain quartz, muscovite, biotite, and plagioclase in all fields. The mean values estimated via conventional thermobarometry and winTWQ are presented in Fig. 8.

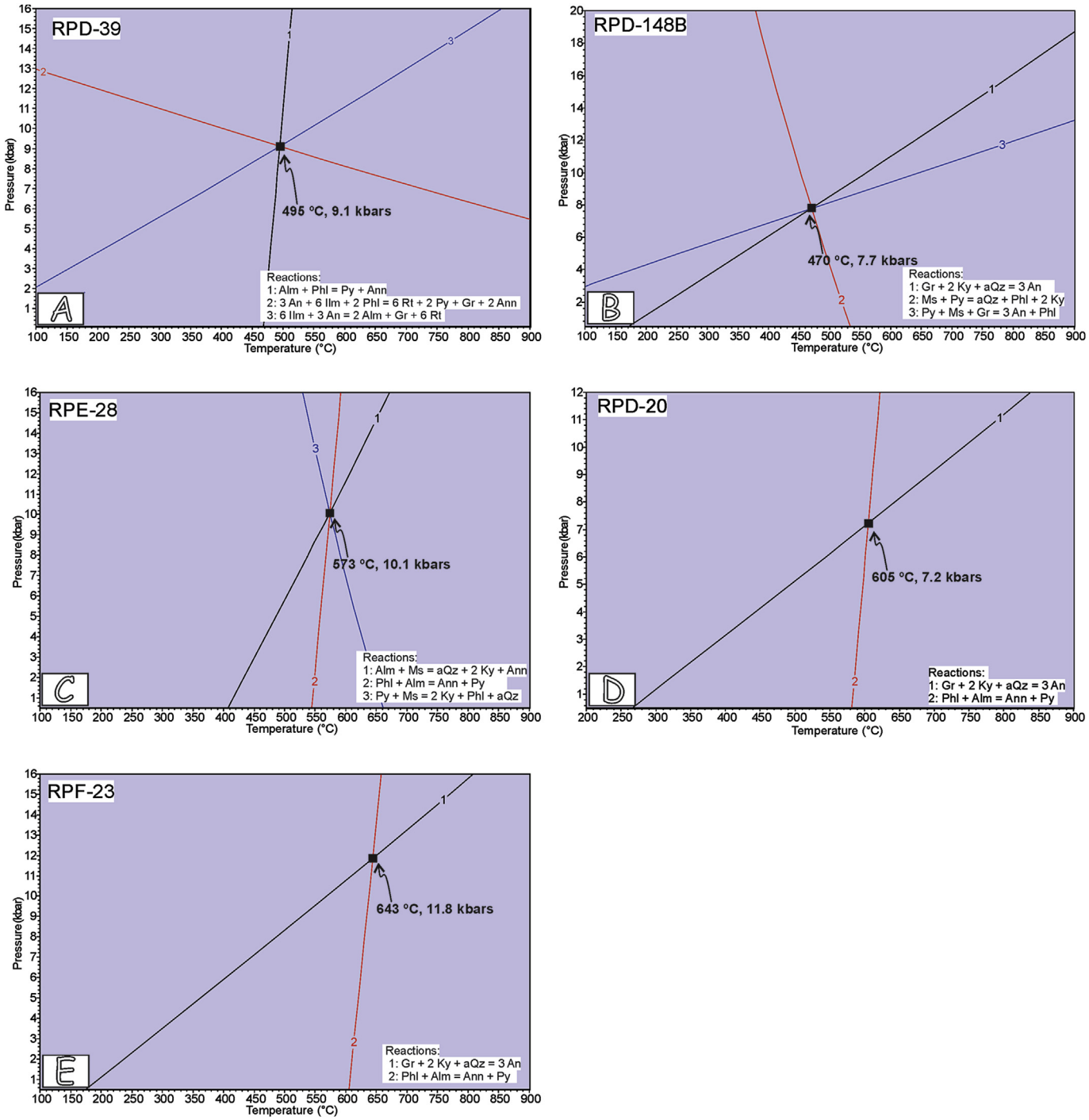

Fig. 7. Equilibrium curves obtained with the winTWQ (version 2.32) software. The intersection between the curves provides the measured P-T value for each sample. The reactions utilized for the construction of the curves also shown in this figure.

Rutile is stable in sample RPF-23 in all fields, under pressures above ~7.6 kbar, whereas ilmenite disappears totally under the same conditions (Fig. 8a). Kyanite stability fields occur between 9.2 and 10.8 kbar and 640-700 °C; the fields coincide with the disappearance of chloritoid. Garnet is stable in practically all fields, except in some small bivariant fields under low pressures and temperatures (Fig. 8a). The rutile-kyanite-plagioclase-garnet-muscovite-biotite-quartz paragenesis of sample RPF-23 is located in a wide P-T field, as indicated in the pseudosection of Fig. 8a. Thus, due to the absence of staurolite and considering that the P-T conditions estimated via thermobarometry were of the order of 643 °C and 11.8 kbar (Fig. 7e), it is reasonable to admit upper amphibolite facies conditions for this sample.

Regarding the pseudosection for sample RPE-28, the replacement of ilmenite by rutile occurs in fields of pressures above ~8.5 kbar, and in the whole pseudosection temperature interval. The pressure conditions also coincide with the fields in which garnet is stable. Kyanite occurrence depends on the breakdown of staurolite and chloritoid (Fig. 8b). Under the microscope, it is possible to see the staurolite breakdown reaction in the St-Ky-Grt-

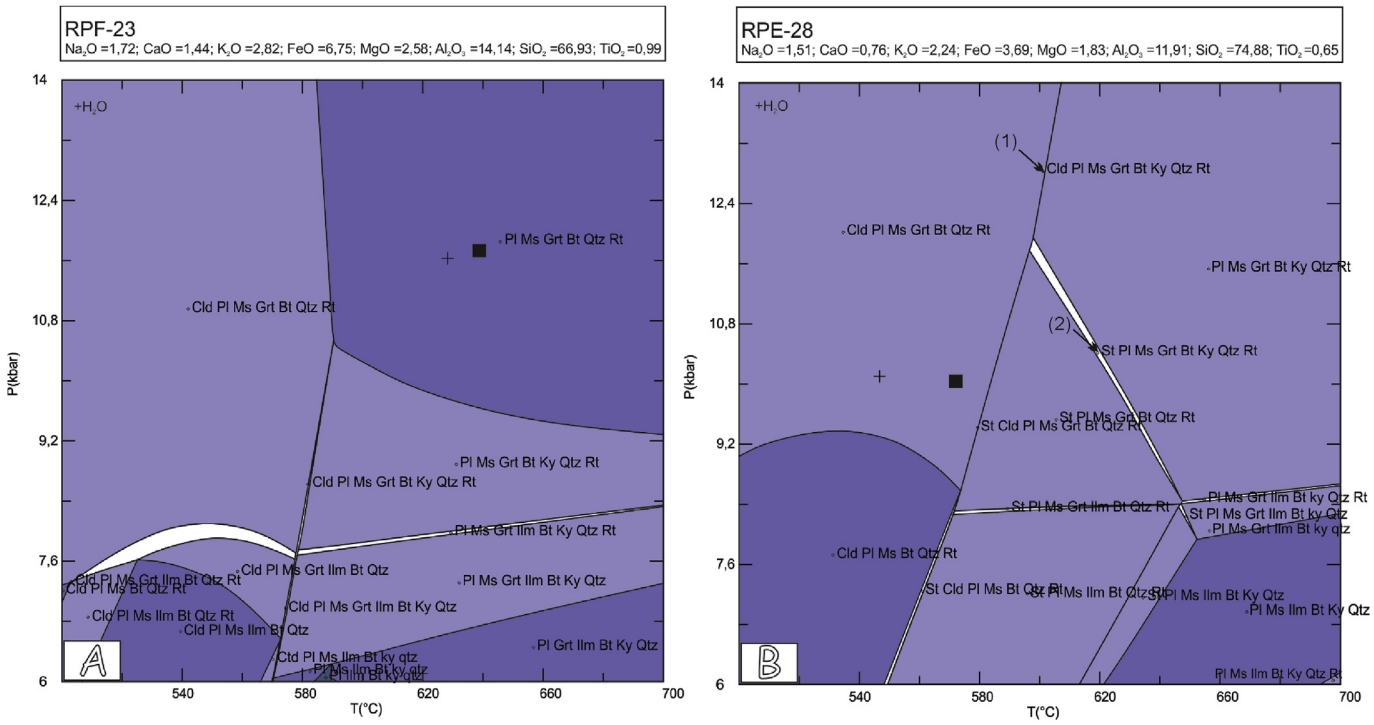

Fig. 8. P-T pseudosection for samples RPF-23 and RPE-28, calculated with PERPLE_X software in the NCKFMASHT chemical system. In this pseudosections also were ploted the P-T values obtained with the winTWQ software (in closed square) and with GPT worksheet (in "+"). Arrows (1) and (2) in Fig. 8b show two bivariant fields. In the first, there is the Cld-Grt-Bt-Ky association, and in the second Cld disappears and St appears, forming the St-Grt-Bt-Ky association.

Bt schist (sample RPE-28) (Fig. 4d and f). Thus, it is possible to assume that the rutile-plagioclase-kyanite-garnet-biotite-muscovite-quartz mineral assemblage is in equilibrium under lower amphibolite facies. In the pseudosection, the field rutile-plagioclase-garnet-biotite-kyanite presented in Fig. 8b contains the described paragenesis. The metamorphic peak conditions established by means of the winTWQ software revealed equilibrium at 573 °C and 10.1 kbar. Therefore, only the pressure values are compatible with the peak paragenesis suggested by the modeled pseudosection, whereas the temperature interval presented a difference of *ca.* 100 °C (Fig. 8b).

6. Discussions and conclusions

Mineral assemblages constituted of rutile-staurolite-muscovite-biotite-garnet-quartz (St-Grt-Bt schist, sample RPF-39), rutile-kyanite-garnet-biotite-quartz (Ky-Grt-Bt paragneiss, sample RPD-148B), kyanite-garnet-biotite-quartz (St-Ky-Grt-Bt schist, sample RPE-28), and rutile-kyanite-garnet-muscovite-biotite-quartz (Ky-Grt-Bt schist, samples RPD-20 and RPF-23) are typically formed under amphibolite facies conditions (Bucher and Grapes, 2011). Garnet with deformed cores, in association with staurolite, and partially replaced by muscovite and biotite indicate part of a higher temperature assemblage (Fig. 9a). Thus, this association suggests progressive metamorphism in the amphibolite facies conditions, however, the coexistence of chloritoid and staurolite indeed points to transition between the upper greenschist facies to the lower amphibolite facies (Spear and Cheney, 1989; Bucher and Grapes, 2011). P-T conditions calculated with GPT and winTWQ for this mineral assemblage were 10.6 kbar and 458 °C, and 9.1 kbar and 495 °C, respectively, which are compatible with the metamorphic conditions suggested for this rock (Table 6 and Fig. 7a). Progressive metamorphism in the rock may also be revealed from the inclusion-rich garnet porphyroblast, and from zoning in some garnet crystals. For example, in Fig. 5a it is observed that the garnet core is enriched in the grossular molecule, whereas the rims are enriched in the almandine molecule.

In the Ky-Grt-Bt schist (sample RPE-28) the textural and mineral relations presented in the pretrographic section suggest that garnet, staurolite, and kyanite porphyroblasts are relics of a previous assemblage, most probably pre-metamorphic peak. The minerals contain abundant inclusions that apparently represent matrix minerals incorporated during growth of this porphyroblasts. Mineral equilibrium between St-Ky-Grt indicates metamorphism in the lower to middle amphibolite facies conditions, possibly reaching upper amphibolite facies in the kyanite stability field (Powell and Holland, 1990; Bucher and Grapes, 2011), since it is possible to see kyanite replacing staurolite (Fig. 4d and e) according to reaction (1). Analysis of the free-inclusion rim in garnets suggest higher temperature cristalization phase, related to metamorphic peak. However, chloritoid is also present in the sample in contact (replacing) with biotite (Fig. 9b), which indicates low-grade metamorphism (lower amphibolite facies – post-metamorphic peak). Therefore, reaction (2) could indicates the post-metamorphic peak phase, but in lower amphibolite facies conditions. Thermobarometric calculations for the Ky-Grt-Bt schist indicate mean temperatures of the order of 533 °C (GPT), 573 °C (winTWQ), and mean pressures of 10.1 kbar (winTWQ), 10.1 kbar (GPT) (Table 6 and Fig. 7c). The results are compatible with paragenesis containing kyanite-garnet-staurolite associated with biotite under lower to medium amphibolite facies conditions, implying that the obtained P-T values do not reflect the metamorphic peak conditions. The main argument to lead to this assumption is the fact that kyanite replaces staurolite. In this sense, the garnet rim inclusion-free founded associated with some kyanite crystals records higher temperatures than gerthemormetric calculations. Thus, the lower temperatures revealed by the thermobarometry are due to the homogenization of growth zoning

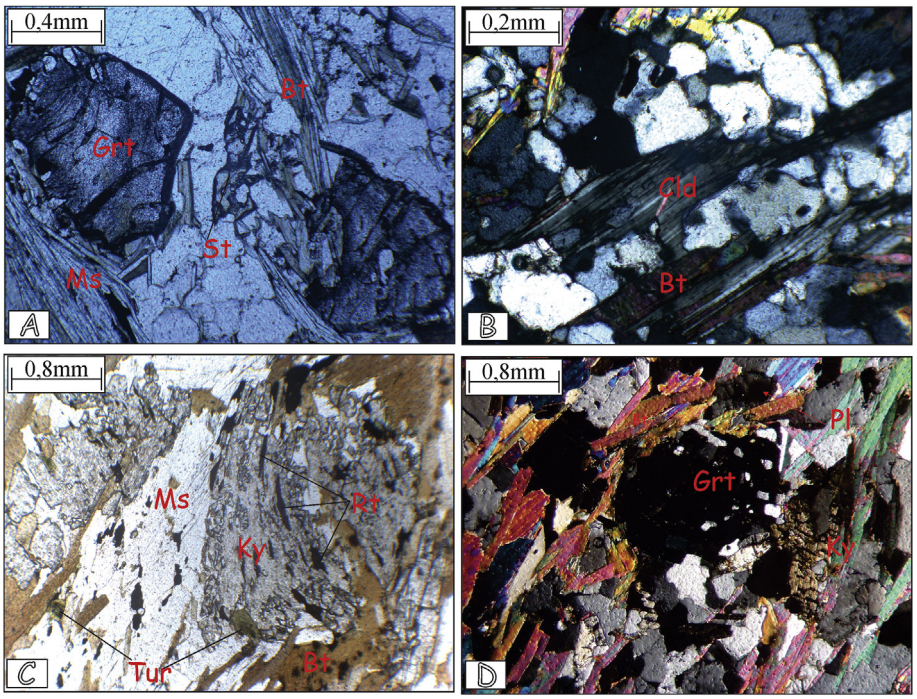

Fig. 9. Indicative mineralogical and textural features of the metamorphic conditions. (a) Sample RPF-39; (b) Sample RPE-28; (c) Sample RPD-148B; (d) Sample RPF-23. (a) Photomicrograph showing the garnet-bioite pair and the staurolite break-up (transmitted light; crossed polars). (b) Chloritoid replacing biotite (transmitted light; crossed polars). (c) Biotite partially replacing kyanite (transmitted light; crossed polars). (d) Photomicrograph with paragenesis composed of garnet-biotite-kyanite-plagioclase (transmitted light; crossed polars).

of garnet at relatively higher temperature of upper amphibolite facies metamorphism and development of retro-grade zoning near the rim as a result of partial re-equilibration with the coexisting phases in response to changing P–T condition (Spear, 1991; Tirone and Ganguly, 2010). The pseudosection modeled for the sample contributes to a better visualization of the progressive character of the metamorphism. There are two bivariant fields in Fig. 8b. In the first, there is the Cld-Grt-Bt-Ky-Ms-Qtz-H_2O association, and in the second Cld disappears and St appears, forming the St-Grt-Bt-Ky association. The fields present P-T intervals compatible with the metamorphic peak (second field), and pre-metamorphic peak (first field) trajectories.

Reaction (1): St + Ms + Qtz = Grt + Als (Ky) + Bt

Reaction (2): Bt + St = Ms + Cld

In the Ky-Grt-Bt paragneiss (Sample RPD-148B), garnet and kyanite porphyroblasts rich in biotite, plagioclase, muscovite, and quartz inclusions were documented and interpreted to represent the pre-peak metamorphic stages. The estimated metamorphic P-T conditions for the sample, seen in the thermobarometry section, display mean values obtained by means of GPT (509 °C and 8.2 kbar), and winTWQ (470 °C and 7.7 kbar) (Table 6 and Fig. 7b). The conditions are compatible with mineral assemblages developed in greenschist facies to lower amphibolite facies along kyanite stability field representing pre-peak metamorphic conditions. However, the Ky-Grt-Bt paragneiss present a partial melting evidence with leucosome mainly constituted of quartz and plagioclase. Additionally, lack of staurolite, plus the chessboard extinction pattern in quartz grains, which indicates deformation in high-grade conditions, it is probable that in this rock P-T conditions reach the upper amphibolite facies (Kruhl, 1996). The statement agrees with the paragenesis founded in petrographic section. Futhermore, kyanite destabilization is presented in Fig. 9c, where the mineral is very irregular with ameboid rims, and partially replaced by muscovite and biotite. Thus, kyanite represents part of a previous assemblage. The textural relationship indicates post-metamorphic peak conditions, probably associated with a decompression phase related to tectonic exhumation. Unfortunately, the thermobarometric data obtained for this sample only recorded the mineral conditions developed in pre-peak metamorphic phase.

The Ky-Grt-Bt schist (samples RPD-20 and RPF-23) shows progressive metamorphic conditions under higher temperatures and pressures. The lack of staurolite, plus the paragenesis composed of garnet-biotite-kyanite suggests, according to reaction (1) (Fig. 9d), staurolite breakdown (Powell and Holland, 1990) under upper amphibolite facies conditions, similarly to what is recorded in sample RPE-28. The P-T estimates for sample RPD-20 were 608 °C and 7.7 Kbar (GPT), 605 °C and 7.2 kbar (winTWQ). It is noteworthy that, regarding the pressure values calculated for the rocks, sample RPF-23 yielded much higher pressure values (11.58–11.8 kbar) when compared to sample RPD-23 (7.2–7.66 kbar). However, the temperature, despite slightly higher than in sample RPF-23, did not vary much (see Table 6 and Fig. 7d and e). It is possible that isothermal decompression took place in a certain P-T interval, assuming a clockwise metamorphic trajectory. It must be considered that the Zr thermometry calculations for rutile yielded slightly higher temperatures for sample RPD-20, when compared to sample RPF-23, but the values are within the acceptable error for geothermometers. It is seen very close P-T conditions with mineral assemblages characteristic of the metamorphic peak at the upper amphibolite facies in a pseudosection prepared for sample RPF-23 (Fig. 8b), which precisely showed the fields where rutile is stable.

Based on the obtained data, a P-T trajectory for the studied rocks is presented in Fig. 10. A clockwise trajectory was established taking place as a function of the metamorphism progressive character evidenced by the textural relationships, thermobarometric data,

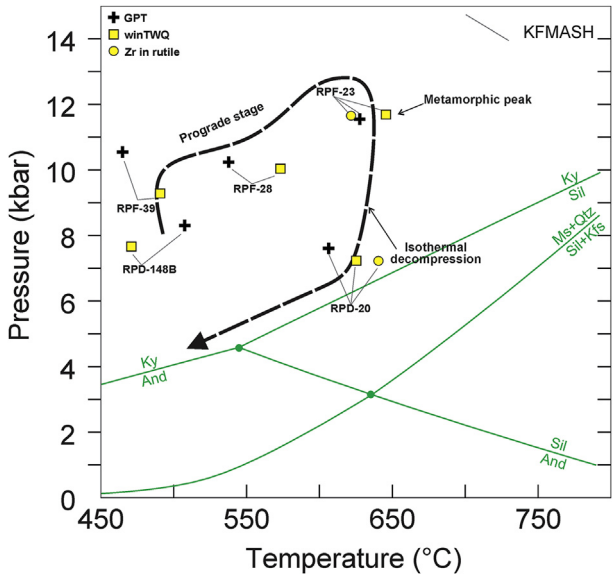

Fig. 10. P-T plot in a petrogenetic grid showing the calculated values by the methods used in this study. The grid also shows a clockwise path for the metamorphism, with three possible phases or stages: (1) Progressive stage; (2) metamorphic peak; and (3) isothermal decompression. The grid was adapted from Spear et al. (2008).

and modelling with pseudosections. P-T clockwise trajectory metamorphism with the involvement of decompression is usually associated with collisional tectonic settings, either related to subduction or to continental collisions (Brown, 2001, 2007; Harley, 2008). It implies that this portion of the Riacho do Pontal Orogen may have undergone subduction/collision processes with subsequent uplift/exhumation. Although thinking about tectonic exhumation would be conjectural, we must understand that pressures of 12 kbar were reached during suggested metamorphic-peak, whereas the lower pressures were 7 kbar, along a clockwise path (Fig. 10). It implies a volumetric decrease of almost twice in magnitude of the continental crust.

In this sense, the Santa Filomena Complex in the Riacho do Pontal Orogen belongs to the Borborema Province, which is attributed to a regional branched system of orogens, whose final structuration took place in the Late Neoproterozoic during the Brasiliano Orogeny (Ediacaran) (Brito Neves et al., 2000; Van Schmus et al., 2008, 2008). The Brasiliano Orogeny affected the whole Borborema Province, and it was responsible for the low-to high-grade metamorphism, deposition of syn-orogenic basins, emplacement of granitic plutons, and the development of continental-scale shear zones (Guimarães et al., 2012; Caxito et al., 2014a). The regional metamorphism and the main deformation started *ca*. 650-640 Ma, whereas the shear zones started in 590–595 Ma (Neves, 2003). The most powerful evidences of the Brasiliano Orogeny record in the Riacho do Pontal Orogen is the syn-collisional orthogneisses of the Rajada Suite (Caxito, 2013; Brito Neves et al., 2015). Brito Neves et al. (2015) presented a U-Pb discordia for the Rajada Suite orthogneisses, which represents the regional metamorphism climax at 620 ± 8 Ma in the Riacho do Pontal Orogen.

Regarding the Santa Filomena Complex, geochronological data that support this regional metamorphism are still missing. Brito Neves et al. (2015) and Santos et al. (2017) based on U-Pb dating of detrital zircon grains from the Santa Filomena Complex metasedimentary rocks, obtained a maximum sedimentation age of 750 Ma. However, they could not obtain precise ages for the regional Brasiliano metamorphism. Despite the doubt regarding the chronology of the regional metamorphism, it is probable that the metamorphic conditions with climax in the upper amphibolite facies were only reached in the Brasiliano Orogeny. The regional tectonic fabric of the Santa Filomena Complex, with an approximately NE-SW to ENE-WSW trend, seems to be characteristic of those of the Brasiliano described in other Borborema Province portions (Neves, 2003; Amaral et al., 2012; Archanjo et al., 2013; Garcia et al., 2014). However, more detailed geochronologic studies are required in order to elucidate the chronology of the regional metamorphism in the areas where it reached amphibolite facies conditions, and the Brasiliano structuration in the Santa Filomena Complex. Futhermore, is also necessary pay more attention for the relationships between metamorphism, melting, and fabric formation, in order to unravel the complex tectonic history of the Riacho do Pontal Orogen.

Acknowledgments

The authors are grateful to FAPESP – Fundação de Amparo a Pesquisa do Estado de São Paulo for field work and laboratory support (Proc. 2014/03275-3). WSA is especially grateful to CNPq – Conselho Nacional de Desenvolvimento Científico e Tecnológico, for granting him a research scholarship. FHS is grateful to Dr. Daniel Françoso Godoy for the support in the acquirement of the mineral chemical data. We appreciate the comments and suggestions of the reviewers, Professor Reinhardt A. Fuck, an anonymous reviewer and Editor-in-Chief handling by James Kellogg.

References

Alkmim, F.F., 2001. Assembling West Gondwana in the neoproterozoic: clues from the São Francisco craton region. Brazil. Geology 29, 319–322.
Almeida, F.F.M., Hasui, Y., Brito-Neves, B.B., Fuck, R.A., 1981. Brazilian structural provinces: an introduction. Earth Sci. Rev. 17, 1–29.
Amaral, W.S., Santos, T.J.S., Wernick, E., Nogueira Neto, J.A., Dantas, E.L., Matteini, M., 2012. High-pressure granulites from Cariré, Borborema Province, NE Brazil: tectonic setting, metamorphic conditions and U Pb, Lu Hf and Sm Nd geochronology. Gondwana Res. 22, 892–909.
Angelim, L.A.A., 1988. Programa Levantamentos Geológicos Básicos Do Brasil-PLGB, Carta Geológica, Carta Metalogenética, Escala 1:1.00000, Folha SC.24-v-a-iii. Santa Filomena, Estados de Pernambuco e Piauí. DNPM/CPRM, 146 pp.
Angelim, L.A.A., Kosin, M., 2001. Aracaju NW: Folha SC.20-V Estados da Bahia, Pernambuco e Piauí Escala 1:500.000. Programa Levantamentos Geológicos Básicos do Brasil-PLGB. CPRM, Rio de Janeiro, 1 CD-Rom.
Araujo, C.E.G., Rubatto, D., Hermann, J., Cordani, U.G., Caby, R., Basei, M.A.S., 2014. Ediacaran 2,500-km-long synchronous deep continental subduction in the West Gondwana Orogen. Nat. Commun. 5, 5198.
Archanjo, C.J., Viegas, L.G.F., Helena, M., Hollanda, B.M., Souza, L.C., Liu, D., 2013. Timing of the HT/LP transpression in the neoproterozoic seridó belt (Borborema province, Brazil): constraints from U-Pb (SHRIMP) geochronology and implications for the connections between NE Brazil and West Africa. Gondwana Res. 23, 701–714.
Berman, R.G., 1988. Internally-consistent thermodynamic data for minerals in the system Na2O–K2O–CaO–MgO–FeO–Fe2O3–Al2O3–SiO2–TiO2–H2O–CO2. J. Petrol. 29, 445–522.
Berman, R.G., 1991. Thermobarometry using multi-equilibrium calculations: a new technique with petrological applications. Can. Mineral. 29, 833–855.
Berman, R.G., 2007. winTWQ (version 2.3): a software package for performing internally-consistent thermobarometric calculations. Geol. Surv. Canada. Open File, 5462, 41p, edn 2.34.
Bizzi, L.A., Schobbenhaus, C., Gonçalves, J.H., Baars, F.J., Delgado, I.M., Abram, M.D., Neto, R.L., Matos, G.M.M., Santos, J.O.S., 2007. Mapa Geológico Do Brasil, Escala 1:2.500.000. MME-CPRM, Brasília (CD-ROM).
Brito Neves, B.B., 1975. Regionalização Geotectônica do Pré-Cambriano Nordestino. Tese de Doutorado. Instituto de Geociências, Universidade de São Paulo, São Paulo, 198 pp.
Brito Neves, B.B., Santos, E.J., Van Schmus, W.R., 2000. Tectonic history of the Borborema province, northeast Brazil. In: Cordani, U.G., Milani, E.J., Thomaz Filho, A., Campos, D.A. (Eds.), 31st International Geological Congress. Tectonic Evolution of South America, Rio de Janeiro, pp. 151–182.
Brito Neves, B.B., Van Schmus, W.R., Angelim, L.A.A., 2015. Contribuições ao conhecimento da evolução geológica do Sistema Riacho do Pontal - PE, BA, PI. Geol. Usp. Série Científica 15, 57–93.
Brown, M., 2001. From microscope to mountain belt: 150 years of petrology and its contribution to understanding geodynamics, particularly the tectonics of

orogens. J. Geodyn. 32, 115–164.
Brown, M., 2007. Metamorphic conditions in orogenic belts: a record of secular change. Int. Geol. Rev. 49, 193–234.
Brown, M., 2014. The contribution of metamorphic petrology to understanding lithosphere evolution and geodynamics. Geoscience Frontiers 5, 553–569.
Bucher, K., Grapes, M., 2011. Petrogenesis of Metamorphic Rocks. Springer-Verlag, eighth ed. 428 pp.
Caby, R., 1989. Precambrian terranes of the Benin-Nigeria and northeast Brazil and the late proterozoic south atlantic fit. Geological Society of America Special Paper 230, 145–158.
Castaing, C., Feybesse, L., Thiéblemont, D., Triboulet, C., Chèvremont, P., 1994. Palaeogeographical reconstructions of the Pan-African/Brasiliano orogen: closure of an oceanic domain or intracontinental convergence between major blocks? Precambrian Res. 69, 327–344.
Caxito, F.A., 2013. Geotectônica e evolução crustal das faixas Rio Preto e Riacho do Pontal, estados da Bahia, Pernambuco e Piauí. Tese de Doutorado. Instituto de Geociências, Universidade Federal de Minas Gerais, 288 pp.
Caxito, F.A., Uhlein, A., Dantas, E.L., 2014a. The Afeição augen-gneiss suite and the record of the cariris velhos orogeny (1000-960 Ma) within the Riacho do pontal fold belt, NE Brazil. J. S. Am. Earth Sci. 51, 12–27.
Caxito, F., Uhlein, A., Stevenson, R., Uhlein, G.J., 2014b. Neoproterozoic oceanic crust remnants in northeast Brazil. Geology 42, 387–390.
Caxito, F.A., Uhlein, A., Dantas, E.L., Stevenson, R., Salgado, S.S., Dussin, I., Sial, A.N., 2016. A complete Wilson cycle recorded within the Riacho do pontal orogen, NE Brazil: implications for the neoproterozoic evolution of the Borborema province at the heart of West Gondwana. Precambrian Res. 282, 97–120.
Connolly, J.A.D., 2005. Computation of phase equilibria by linear programming: a tool for geodynamic modeling and its application to subduction zone decarbonation. Earth Planet Sci. Lett. 236, 524–541.
Dantas, E.L., Souza, Z.S., Wernicke, E., Hackspacher Martin, H., Xiaodong, L., 2013. Crustal growth in the 3.4 to 2.7 Ga São José de Campestre Massif, Borborema Province, NE Brazil. Precambrian Res. 227, 120–156.
De Wit, M.J., Brito Neves, B.B., Trouw, R.A.J., Pankhurst, R.J., 2008. Pre-Cenozoic correlations across the South Atlantic region: “the ties that bind”. In: Pankhurst, R.J., Trouw, R.A.J., Brito Neves, B.B., De Wit, M.J. (Eds.), West Gondwana: Pre-cenozoic Correlations across the Atlantic Region: Geological Society, vol 294. Special Publications, London, pp. 1–8.
Fetter, A.H., 1999. U-pb and Sm-nd Geochronological Constraints on the Crustal Framework and Geologic History of Ceará State, NW Borborema Province, NE Brazil: Implications for the Assembly of Gondwana. The University of Kansas. Ph.D. Thesis.
Ganguly, J., Saxena, S.K., 1984. Mixing properties of aluminosilicate garnets: constraints from natural and experimental data, and applications to geothermometry. Am. Mineral. 69, 88–97.
Garcia, M.G., Santos, T.J.S., Amaral, W.S., 2014. Provenance and tectonic setting of Neoproterozoic supracrustal rocks from the Ceará Central Domain, Borborema Province (NE Brazil): constraints from geochemistry and detrital zircon ages. Int. Geol. Rev. 56, 481–500.
Guimarães, I.P., Van Schmus, W.R., Brito Neves, B.B., Bittar, S.M.B., Silva Filho, A.F., Armstrong, R., 2012. U-Pb zircon ages of orthogneisses and supracrustal rocks of the Cariris Velhos belt: onset of Neoproterozoic rifting in the Borborema Province, NE Brazil. Precambrian Res. 192–195, 52–77.
Harley, S.L., 2008. Refining the P–T records of UHT crustal metamorphism. J. Metamorph. Geol. 26, 125–154.
Hodges, K.V., Crowley, P.D., 1985. Error estimation and empirical geothermobarometry for pelitic systems. Am. Mineral. 70, 702–709.
Hodges, K.V., Spear, F.S., 1982. Geothermometry, Geobarometry and the Al2SiO5 Triple Point at Mt. Moosilauke. New Hampshire. American Mineralogist, 67, I I l8-l 134.
Holdaway, M.J., Lee, S.M., 1977. Fe-mg Cordierire Stability in High Grade Pelitic Rocks Based on Experimental, Theoretical and Natural Observations Contributions to Mineralogy and Petrology, vol 63, pp. 175–198.
Holdaway, M.J., Dutrow, B.L., Hinton, R.W., 1988. Devonian and Carboniferous metamorphism in west–central Maine: the muscovite–almandine geobarometer and the staurolite problem revised. Am. Mineral. 73, 20–47.
Holland, T.J.B., Powell, R., 1991. A compensated-Redlich–Kwong (CORK) equation for volumes and fugacities of CO_2 and H_2O in the range 1 bar to 50 kbar and 100–1600 °C. Contrib. Mineral. Petrol. 109, 265–273.
Holland, T.J.B., Powell, R., 1998. An internally-consistent thermodynamic dataset for phases of petrological interest. J. Metamorph. Geol. 16, 309–344.
Indares, A., Martignole, J., 1985. Biotite-garnet thermometry in the granulite facies: the influence of Ti and Al in biotite. Am. Mineral. 70, 272–278.
Jardim de Sá, E.F., Macedo, M.H.F., Fuck, R.A., Kawashita, K., 1992. Terrenos proterozóicos na província Borborema e a margem norte do Cráton do São Francisco. Rev. Bras. Geociencias 22, 472–480.
Koziol, A.M., 1989. Recalibration of garnet-plagioclase-Al2SiO5-quartz (GASP) geobarometer and applications to natural parageneses. Eos, Trans. Am. Geophys. Union 70, 493.
Kretz, R., 1983. Symbols for rock-forming minerals. Am. Mineral. 68, 277–279.
Kruhl, J.H., 1996. Prism- and basal-plane parallel subgrain boundaries in quartz; a microstructural geothermobarometer. J. Metamorph. Geol. 14, 581–589.
Luvizotto, G.L., Zack, T., 2009. Nb and Zr behavior in rutile during high-grade metamorphism and retrogression: an example from the Ivrea-Verbano zone. Chem. Geol. 261 (3–4), 303–317.
Luvizotto, G.L., Zack, T., Meyer, H.P., Ludwig, T., Triebold, S., Kronz, A., Münker, C., Stockli, D.F., Prowatke, S., Klemme, S., Jacob, D.E., von Eynatten, H., 2009. Rutile crystals as potential trace element and isotope mineral standards for microanalysis. Chem. Geol. 261 (3–4), 346–369.
Marimon, M.P.C., 1990. Petrologia e litogeoquímica da seqüência plutono-vulcanosedimentar de Brejo Seco. Município de São João do Piauí. Instituto de Geociências, Universidade Federal da Bahia. Dissertação de Mestrado, 102 pp.
Murphy, J.B., Nance, R.D., 2003. Do supercontinents introvert or extrovert? Sm-Nd isotopic evidence. Geology 31, 873–876.
Neves, S.P., 2003. Proterozoic history of the Borborema province (NE Brazil): correlations with neighboring cratons and Pan-African belts and implications for the evolution of western Gondwana. Tectonics 22, 1031.
Neves, S.P., 2011. Atlantica revisited new data and thoughts on the formation and evolution of a long-lived continent. Int. Geol. Rev. 53, 1377–1391.
Neves, S.P., 2015. Constraints from zircon geochronology on the tectonic evolution of the Borborema Province (NE Brazil): widespread intracontinental Neoproterozoic reworking of a Paleoproterozoic accretionary orogeny. J. S. Am. Earth Sci. 58, 150–164.
Neves, S.P., Mariano, G., 1999. Assessing the tectonic significance of a large-scale transcurrent shear zone system: the Pernambuco lineament, northeastern Brazil. J. Struct. Geol. 21, 1369–1383.
Newton, R.C., Haselton, H.T., 1981. Thermodynamics of the garnet-plagioclase-Al2SiO5-quartz geobarometer. In: Newton, R.C., Navrotsky, A., Wood, B.J. (Eds.), Thermodynamics of Minerals and Melts. Springer, New YorD, pp. 129–145.
Oliveira, R.G., 1998. Arcabouço geotectônico da região da Faixa Riacho do Pontal, Nordeste do Brasil: dados aeromagnéticos e gravimétricos. Dissertação (Mestrado) (São Paulo: Instituto de Geociências – USP).
Oliveira, R.G., 2008. Arcabouço geofísico, isostasia e causas do magmatismo Cenozóico da Província Borborema e de sua margem continental (Nordeste do Brasil). PhD thesis. Universidade Federal do Rio Grande do Norte, 411 pp.
Oliveira, E.P., Windley, B.F., Araújo, M.N.C., 2010. The Neoproterozoic Sergipano orogenic belt, NE Brazil: a complete plate tectonic cycle in western Gondwana. Precambrian Res. 181, 64–84.
Perpetuo, M.P., Amaral, W.S., Costa, F.C., Uchoa Filho, E.C., Sousa, D.F.M., 2016. Geochemistry of the Serra das Melancias Pluton in the Serra da Aldeia Suite: a classic post-collisional high Ba-Sr granite in The Riacho do Pontal Fold Belt, NE Brazil. Braz. J. Geol. 46 (2), 221–237.
Powell, R., Holland, T., 1990. Calculated mineral equilibria in the pelite system, KFMASH (K_2O-FeO-MgO-Al_2O_3-SiO_2-H_2O. Am. Mineral. 75 (3–4), 367–380.
Reche, J., Martinez, F.J., 1996. GPT: an Excel spreadsheet for thermobarometric calculations in metapelitic rocks. Comput. Geosci. 22 (7), 775–784.
Salgado, S.S., Ferreira Filho, C.F., Caxito, F.A., Uhlein, A., Dantas, E.L., Stevenson, R., 2016. The Ni-Cu-PGE mineralized Brejo Seco mafic-ultramafic layered intrusion, Riacho do pontal orogen: onset of tonian (ca. 900 Ma) continental rifting in northeast Brazil. J. S. Am. Earth Sci. 70, 324–339.
Santos, E.J., Brito Neves, B.B., 1984. Província Borborema. In: Almeida, F.F.M., Hasui, Y. (Eds.), O Pré-cambriano Do Brasil. Edgar Blucher Ltd, São Paulo, 123–186 pp.
Santos, E.J., Van Schmus, W.R., Kozuch, M., Brito Neves, B.B., 2010. The Cariris Velhos tectonic event in northeast Brazil. J. S. Am. Earth Sci. 29, 61–76.
Santos, F.H., Amaral, W.S., Uchôa Filho, E.C., Martins, D.T., 2017. Detrital zircon U–Pb ages and whole-rock geochemistry of the Neoproterozoic Paulistana and Santa Filomena complexes, Borborema Province, northeastern Brazil: implications for source area composition, provenance, and tectonic setting. Int. Geol. Rev. 59 (15), 1861–1884.
Spear, F.S., 1991. On the interpretation of peak metamorphic temperatures in light of garnet diffusion during cooling. J. Metamorph. Geol. 9, 379–388.
Spear, F.S., Cheney, J.T., 1989. A petrogenetic grid for pelitic schists in the system SiO_2-Al_2O3-FeO-MgO-K_2O-H_2O. Contrib. Mineral. Petrol. 101 (2), 149–164.
Spear, F.S., Cheney, J.T., Pyle, J.M., Harrison, T.M., Layne, G., 2008. Monazite geochronology in central New England: evidence for a fundamental terrane boundary. J. Metamorph. Geol. 26, 317–329.
Thompson, A.B., 1976. Mineral reaction in pelitic rocks: I. Prediction of P–T–X (Fe–Mg) phase relations. II. Calculation of some P–T–X (Fe–Mg) phase relations. Am. J. Sci. 276, 401–454.
Tirone, M., Ganguly, J., 2010. Garnet compositions as recorders of P-T-t history of metamorphic rocks. Gondwana Res. 18, 138–146.
Tomkins, H.S., Powell, R., Ellis, D.J., 2007. The pressure dependence of the zirconium-in rutile thermometer. J. Metamorph. Geol. 25 (6), 703–713.
Torsvik, T.H., Cocks, L.R.M., 2013. Gondwana from top to base in space and time. Gondwana Res. 24, 999–1030.
Uhlein, A., Caxito, F.A., Sanglard, J.C.D., Uhlein, G.J., Suckau, G.L., 2011. Estratigrafia e tectônica das faixas neoproterozoicas da porção norte do Cráton do São Francisco. Geonomos 19 (2), 8–31.
Van Schmus, W.R., Oliveira, E.P., Silva Filho, A.F., Toteu, F., Penaye, J., Guimarães, I.P., 2008. Proterozoic Links between the Borborema Province, NE Brazil, and the Central African Fold Belt. Geological Society, vol 294. Special Publications, London, pp. 69–99.
Vauchez, A., Neves, S.P., Caby, R., Corsine, M., Egydio-Silva, M., Arthaud, M., Amaro, V., 1995. The Borborema shear zone system, NE Brazil. J. S. Am. Earth Sci. 8, 247–266.
Viegas, L.G.F., Archanjo, C.J., Hollanda, M.H.B.M., Vauchez, A., 2014. Microfabrics and zircon U-Pb (SHRIMP) chronology of mylonites from the Patos shear zone (Borborema Province, NE Brazil). Precambrian Res. 243, 1–17.
Zack, T., Von Eynatten, H., Kronz, A., 2004. Rutile geochemistry and its potential use in quantitative provenance studies. Sediment. Geol. 171.1, 37–58.